Chem Soc Rev

RSC Publishing

REVIEW ARTICLE

View Article Online
View Journal | View Issue

Cite this: *Chem. Soc. Rev.*, 2013, **42**, 2963

Quantum dot nanoscale heterostructures for solar energy conversion†

Rachel S. Selinsky, Qi Ding, Matthew S. Faber, John C. Wright and Song Jin*

Quantum dot nanoscale semiconductor heterostructures (QDHs) are a class of materials potentially useful for integration into solar energy conversion devices. However, realizing the potential of these heterostructured systems requires the ability to identify and synthesize heterostructures with suitably designed materials, controlled size and morphology of each component, and structural control over their shared interface. In this review, we will present the case for the utility and advantages of chemically synthesized QDHs for solar energy conversion, beginning with an overview of various methods of heterostructured material synthesis and a survey of heretofore reported materials systems. The fundamental charge transfer properties of the resulting materials combinations and their basic design principles will be outlined. Finally, we will discuss representative solar photovoltaic and photoelectrochemical devices employing QDHs (including quantum dot sensitized solar cells, or QDSSCs) and examine how QDH synthesis and design impacts their performance.

Received 10th September 2012

DOI: 10.1039/c2cs35374a

www.rsc.org/csr

1. Introduction

There is an urgent global need for alternative, renewable energy sources for both environmental and economic reasons.[1,2] One extremely appealing source of energy is the sun, which continuously sends enormous quantities of light energy to the surface of the earth. However, harnessing this energy requires the development of inexpensive materials systems capable of harvesting sunlight by efficiently capturing photon energy and then quickly separating and collecting the photoexcited charge carriers.[3,4] Nanotechnology presents new opportunities to achieve higher solar energy conversion efficiencies at lower costs, and in particular, quantum dot nanoscale heterostructures (QDHs) that facilitate charge transfer are very promising for such applications.[5–9]

1.1 Current solar energy conversion technologies

There are two principal approaches for harnessing solar energy using semiconductor materials: photovoltaic (PV) and photoelectrochemical (PEC) solar energy conversion.[1,2,4,9] When semiconductors

Department of Chemistry, University of Wisconsin-Madison, 1101 University Avenue, Madison, Wisconsin 53706, USA. E-mail: jin@chem.wisc.edu

† Part of the chemistry of functional nanomaterials themed issue.

Rachel S. Selinsky

Rachel Sarah Selinsky received her BA in chemistry and art from Williams College in 2006. *She obtained her PhD in chemistry under the supervision of Prof. Song Jin at the University of Wisconsin-Madison in* 2012, *investigating the design and synthesis of magnetic nanocrystals and quantum dot heterostructures. Her research interests include nanoscale materials for solar energy conversion and cultural heritage science.*

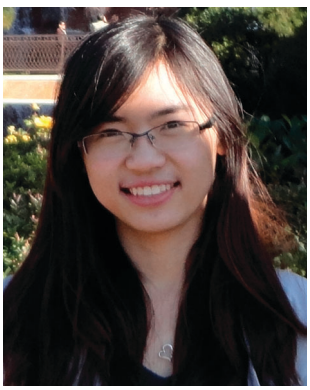

Qi Ding

Qi Ding studied Chemistry at Shandong University, China, graduating with a BS degree in 2011. *She is currently a graduate student at the University of Wisconsin-Madison under the supervision of Prof. Song Jin. Her research is mainly focused on the synthesis, characterization, and solar energy applications of quantum dot nanoscale heterostructures.*

are illuminated, photons with energy greater than the material's band gap are absorbed, resulting in the excitation of an electron from the valence band to the conduction band to create an electron–hole pair, or exciton. PV devices typically generate electricity through charge carrier separation across a homo- or heterojunction between doped semiconductors.[10] Photovoltaic technology has been commercialized and has found relatively large-scale device deployment; however, intense academic and industrial research toward achieving higher efficiencies and lower costs is ongoing.[11] In PEC devices, ionic charge carriers pass between the cathode and anode through a liquid electrolyte medium, participating in reduction and oxidation reactions at the respective electrode–electrolyte interfaces.[12] The rate of charge separation in these reactions is dictated by the space charge layer at each electrode interface. PEC devices can operate as regenerative PV devices, in which a redox couple in the electrolyte solution can shuttle holes (or electrons) from the photoelectrode to the counter electrode, resulting in electrical current.[12] The popular dye-sensitized solar cells (DSSCs)[13] operate in this regenerative mode, as do the liquid-junction quantum dot-sensitized solar cells (QDSSCs)[6,14–18] that will be discussed in this review. PEC devices can also operate as photosynthetic cells, where photoexcited electrons and holes can be used to generate chemical fuels through redox reactions, as in the PEC splitting of water and the PEC reduction of CO_2.[19] PEC solar fuel generation remains under development, and mature commercial technologies and widespread applications have not yet been realized.[4] Despite differences in the particular mode of operation between PV and PEC devices, the processes of light absorption, charge separation, and charge collection are common to any solar energy conversion device.

Photovoltaic technologies can be classified into three distinct "generations" based on their efficiency and cost.[20] First-generation PV cells are composed of p–n homojunctions of single-crystalline Si, and they suffer from low efficiency and high manufacturing and installation costs.[11] Single-crystalline Si is an inefficient light absorber due to its indirect band gap. The use of thicker Si films (up to 100 microns) increases light absorption; however, the distance that charge carriers must diffuse without recombining or becoming trapped before reaching the current collector also increases. This demands Si of extremely high purity and crystalline quality. Ultimately, the performance of these single-crystalline Si PV cells must be weighed against their high manufacturing and processing costs.[1,21]

Second-generation PV technologies utilize polycrystalline semiconductor thin films, such as polycrystalline and amorphous Si, CdTe, $CuInSe_2$ (CIS), and $CuIn_xGa_{1-x}Se_2$ (CIGS).[11] They have achieved significant commercial success and showed rapid increase in market share.[21–23] These solar cells are significantly less expensive than single-crystalline PV cells due to reduced materials and processing costs, and increased manufacturing throughput. The quality of these materials is

Matthew S. Faber

Matthew S. Faber received his BS degree in Chemistry from The University of Texas at Dallas in 2008. He is currently a PhD candidate at the University of Wisconsin-Madison under the supervision of Prof. Song Jin. His research is focused on the photovoltaic applications of low-cost, earth-abundant semiconductor materials.

John C. Wright

John C. Wright has a BS degree from Union College (1965), a PhD in physics from Johns Hopkins (1970). He joined the University of Wisconsin-Madison in 1972 and is currently the Andreas C. Albrecht Professor of Chemistry. His research centers on the development of new laser-based spectroscopy methods that increase the selectivity of chemical measurements and the applications of these methods to molecular and materials chemistry. He has been recognized by the American Chemical Society Spectrochemical Analysis Award, Fellowship in the APS and the AAAS, the UW Chancellor's Award for Teaching Excellence, the Benjamin Smith Reynolds Award for Teaching Excellence in Engineering Courses, and the UpJohn Teaching Award in Chemistry.

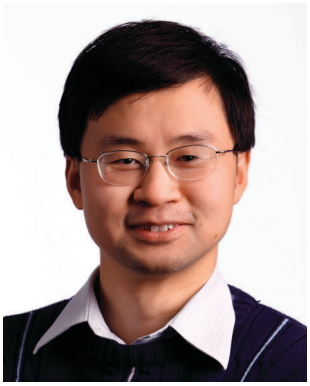

Song Jin

Song Jin received his BS from Peking University (1997) and PhD from Cornell University (2002). He is currently an associate professor of chemistry at the University of Wisconsin-Madison. Dr Jin studies the fundamental formation mechanisms of nanomaterials, especially the dislocation-driven growth of nanomaterials, their novel physical properties, and applications in renewable energy such as solar and thermoelectric energy conversion, and energy storage, nanospintronics, and nanobiotechnology. Some of his recent awards include NSF CAREER Award, MIT Technology Review TR35 Award, ACS ExxonMobil Solid State Chemistry Fellowship, the Alfred P. Sloan Research Fellowship, and Research Corporation SciaLog Award for Solar Energy Conversion.

generally lower than that of the first-generation PV cells, resulting in increased non-radiative recombination and lower overall PV efficiency.[23] All of these single band gap absorber PV cells above are subject to the so-called Shockley–Queisser detailed balance limit of efficiency, which thermodynamically limits the solar energy conversion efficiency to 33% for 1 sun (AM1.5) solar illumination.[24]

Third-generation solar cells incorporate contemporary technologies currently under investigation that aim to lower costs while maintaining high efficiencies, with the potential to exceed the intrinsic efficiency limits of the first- and second-generation solar cells, namely, the Shockley–Queisser theoretical limit. One proposed pathway to overcome the Shockley–Queisser theoretical limit is to use materials capable of producing multiple excited electrons per absorbed photon. In multiple exciton generation (MEG), photon energy in excess of the absorbing material's band gap could be used to generate additional excitons rather than being lost as heat.[25–30] Other proposed designs involve tandem cells, intermediate-band cells, hot-carrier cells, and upconversion.[23,31,32] Chemically synthesized nanomaterials and nanoscale heterostructures provide potential avenues toward achieving the goals of these third-generation solar cells.

1.2 Advantages of nanomaterials for solar energy conversion

Nanomaterials, such as nanocrystals (NCs) or quantum dots (QDs), nanowires (NWs), nanorods (NRs), and heterostructures thereof offer new approaches to efficient photoexcitation and charge separation that promise to improve PV and PEC solar energy conversion by combining novel nanoscale properties with processability and low cost. For example, solution-grown colloidal QDs of PbS, PbSe, CdSe, and other materials can be readily spin-coated or blended with semiconducting polymers and cast on a substrate to fabricate thin-film solar cells.[25,33–39] Importantly, by reducing the dimensions of a semiconductor to the nanoscale, electrons and holes in QDs become quantum confined and the band gap increases.[40,41] Therefore, the size-dependent control of the absorption of quantum-confined materials can enable multi-junction or ''rainbow'' solar cells containing QDs with several sizes and, hence, a range of band gaps (Fig. 1b), each optimized to absorb a particular wavelength of the solar spectrum, enhancing PV performance.[6,42] Furthermore, nanoscale quantum mechanical mechanisms such as MEG[25–30] and hot-electron transfer[31,32] might become feasible in QDs.

One-dimensional (1D) NWs (or microwires) also show promise for solar energy conversion.[43–48] Unlike in conventional planar single-crystalline or thin-film PV or PEC cells, in a NW solar cell, along the long axial dimension of the NW (microns or more) solar light can be sufficiently absorbed while charge carrier separation occurs in the shorter radial direction (tens of nanometers for nanowires).[49] This strategy alleviates problems with defects and impurities that have hindered solar applications of inexpensive, earth-abundant semiconductor materials.[1] NWs are also attractive because they can provide convenient, high-quality electrical connections between components of a solar device system. Additionally, integrating QDs with 1D NWs has also become a fruitful approach for solar energy conversion device design.[50,51] Furthermore, integrating three-dimensional (3D) hierarchical nanostructures, such as complex branching nanowire networks,[52–54] into solar devices could further improve their efficiencies by bridging the mismatched length scales of the various physical processes critical to solar energy conversion: light absorption, charge separation, and carrier collection.[8]

1.3 Quantum dot nanoscale heterostructures and their benefits toward solar energy conversion

The fundamental processes in any PV or PEC energy conversion technology include light absorption and subsequent photoexcitation, charge separation, charge collection, and catalysis (for PEC devices). In heterostructures, charge carrier separation occurs at the heterojunctions and is a crucial step for efficient solar energy conversion. Charge separation is most efficient when heterostructures have suitable band energy alignment and high-quality interfaces. The conventional understanding of charge separation in bulk planar and thin film solar cells involves the classical description of charge carriers moving in electric fields.[10] Nanoscale semiconductor heterostructures containing QDs present new opportunities that could enable much more efficient charge transfer and practical advantages for solar energy conversion applications.

The chemically grown quantum dot nanoscale heterostructures discussed in this review consist of two or more components—each of which will be classified as either a ''donor'' or an ''acceptor'' material—with a shared interface. Generally, charge carriers are generated through photoexcitation in the donor material, and the electrons and holes are separated across the heterojunction with the acceptor material. The ideal donor material

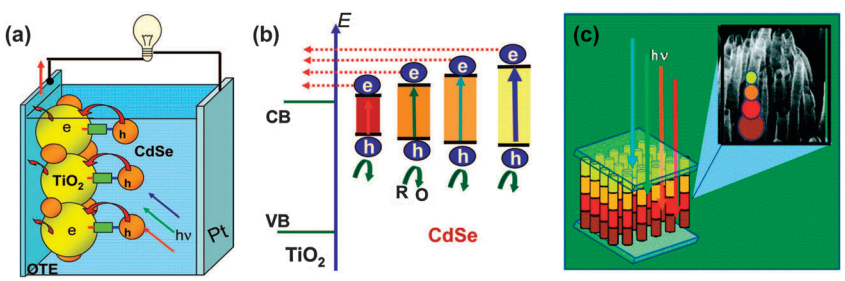

Fig. 1 (a) Schematic representation of a QD-sensitized solar cell (QDSSC), and (b) varying QD band gaps due to quantum confinement, which enables the (c) ''rainbow'' solar cell design. Taken from ref. 6 and 42.

has a high absorption coefficient across the solar spectrum, a band gap suited to the absorption of a large fraction of solar radiation,[10] and conduction and valence band energy levels compatible with those of the acceptor material (see more details on this in Section 4). The acceptor material generally occupies a larger physical volume than the donor, and it forms a conductive pathway for photoexcited charge carriers between the donor and a current-collecting electrode. For convenient integration into solar devices, the acceptor material is typically grown on or otherwise attached to a conductive substrate, which serves as the current collector. These acceptor materials are often wide band gap semiconductors (such as TiO_2, ZnO, or SnO_2),[55] which do not absorb visible and infrared solar photons but have appropriate electronic structure and properties for transferring and transporting charge carriers. The usual progression of QDH synthesis is to first prepare an acceptor material and then to decorate the acceptor with a narrow band gap donor, frequently quantum-confined semiconductor QDs. Ideally, all materials used in solar conversion devices should have low cost and high terrestrial abundance. Expensive or rare materials with unique optical or electronic properties could be employed as donors if they have very large absorption cross-sections and, thus, only a small amount is needed for effective solar light collection. When QDs serve as sensitizers for a wide band gap material, as discussed above, they act as inorganic analogues of the dyes used in dye-sensitized solar cells (DSSCs). Such devices are commonly described as QD-sensitized solar cells (QDSSCs) (see Fig. 1a).

Nanoscale and quantum mechanical effects of the QDHs have many benefits that promote efficient charge transfer in QDHs and are advantageous in solar device applications. First, quantum mechanical effects become important at smaller dimensions as the wave functions of individual materials become delocalized and improve the rate and efficiency of electron transfer.

Second, the band alignment of nanoscale heterostructures can be tuned by adjusting the relative size of the donor–acceptor materials.[6,56,57] Because the band gap and band energy levels of QDs are tunable through quantum confinement,[40,41] modifying their size provides control over band gap, band energy level and alignment with the acceptor to optimize light absorption and charge-transfer efficiency and allow the use of more diverse materials with different optical properties in the QDH solar devices.

Third, the small physical dimensions of QDs allow the formation of epitaxial heterojunctions between largely dissimilar materials because the effects of lattice-mismatch strains are minimized. Optimal charge transfer in QDHs requires high-quality heterojunctions between the donor and acceptor materials. Epitaxial heterostructures that have direct, symmetrically matched crystalline interfaces allow for the most efficient charge transfer. Lattice mismatch, either through symmetry or large differences in lattice parameters, limits possible material combinations and the crystallographic orientations by which the materials can be connected. Such lattice mismatch often significantly limits materials options for bulk semiconductor heterostructures. In bulk, one material can be grown on another with different lattice parameters, but a coherent interface can only be formed within a critical thickness defined by the degree of mismatch.[58,59] Beyond that thickness, dislocations will form, relieving elastic strain but also introducing defects[60] which can act as recombination centers in solar devices and reduce the carrier transfer rate across the heterointerface. In contrast, the dimensions of nanoscale materials can fall far below this critical thickness, allowing for high-quality epitaxial junctions of materials with large lattice mismatches and different lattice orientations.[8,61] As a result, nanoscale heterostructures can often be synthesized between materials that would be incompatible on the macroscale for the preparation of bulk or thin film junctions with a single-crystalline, defect-free interface, thereby broadening the diversity of available materials combinations. For example, it has been shown that NWs of PbS with a cubic rock salt structure can grow epitaxially from the surface of single-crystalline rutile TiO_2.[62] Similarly, PbSe QDs with a rock salt structure can form a heteroepitaxial interface with NWs of hematite (α-Fe_2O_3), which has a hexagonal corundum crystal structure.[63] These examples and others[8,61] demonstrate how more unconventional pairings of semiconductor materials become available for making QDHs. Such high-quality, defect-free heterostructures can facilitate efficient charge transfer for solar energy harvesting and conversion.

QDHs further benefit from the synthetic ability to match the size and length scales of their component materials to the corresponding physical processes involved in solar energy conversion. Specifically, the distance that photogenerated excitons must diffuse to reach the heterojunction can be reduced in order to decrease the likelihood of carrier trapping or recombination at defects, surfaces, or impurities prior to charge transfer.[3] A good example is the use of NWs or 3D NW networks as acceptor materials, where the light absorption and carrier collection directions are orthogonalized, as discussed in the previous section.[8]

Finally, the high surface area of nanostructures allows the use of tunable ligand surface chemistry to control the electronic structure of different parts of a heterostructure and optimize charge transfer. Molecular ligands often coordinate to the crystalline surface of QDs or other nanostructures *via* functional groups and can alter both electronic structure and reactivity. Due to the high surface area-to-volume ratio of QDs, the resulting control over surface states, surface state dynamics, electronic behavior, and stability against Ostwald ripening and oxidation can dominate the overall behavior of the nanostructures. In addition, when QDs form ordered superlattices, porous structures, or randomly packed assemblies, ligands provide a mechanism for maintaining the desired spatial distance between QDs.[3,33] For QDs not joined to an acceptor material by a chemical linker or an epitaxial interface, performance in solar energy conversion devices is strongly influenced by porosity and interparticle distance since they are correlated with the charge transfer rate.

1.4 The scope and structure of the review

Because of the many advantages of QDHs for solar energy conversions (and other applications), they have been intensively investigated over the last few years, which has led to a rapidly expanding body of literature. A broad range of nanoscale

heterostructured materials have been under investigation due to the tunability of materials combinations, interfaces, and electronic structures, which has further spurred various physical property investigations as well as device fabrication and measurement. In this review, we will attempt to provide a critical summary and review of the research progress in developing semiconductor QDHs for solar energy conversion. We will focus the discussion on QDHs containing at least one solution-grown QD material. These QDs are grown either directly on the acceptor material or are separately synthesized and then placed in contact with or molecularly linked to the acceptor material. Such chemically prepared QDHs maintain the benefits of solution-grown QDs: a facile and inexpensive synthesis, compatibility with large scale fabrication, and good reproducibility of physical properties.[9,33,34] Other methods of heterostructure fabrications, such as chemical vapor deposition (CVD), atomic layer deposition (ALD), molecular beam epitaxy (MBE), and other complex, expensive, and low throughput vacuum processing techniques are outside the scope of this review. Therefore, many examples of NW or other nanoscale heterostructures[64–66] formed through vacuum synthesis will not be featured in this review. Chemically synthesized metal–semiconductor nanoscale heterostructures,[67] while potentially useful for catalysis and/or plasmonic applications, and therefore of potential relevance to solar applications, will not be discussed.

The challenges for using QDHs in solar energy conversion are similar to those for any candidate material for solar energy conversion: preparing high quality materials, minimizing defects, controlling surfaces and interfaces, engineering electronic structure, improving charge transfer at various interfaces, and reducing carrier trapping and recombination. Therefore, we will first review the current research progress in the chemical synthesis of QDHs that lead to specific, controlled, and precise heterojunctions. Classification of the basic types of QDHs and how they are prepared are summarized along with a survey of QDHs prepared from a variety of donor QDs and acceptor nanostructures. The study of these QDHs has provided an understanding of the charge and energy transfer processes which are central for optimizing the solar energy conversion process. We will discuss the structural and fundamental characterization methods presently employed to evaluate these materials for use in solar energy conversion. We will focus on the charge transfer properties of these heterostructures that define the novelty and utility of QDHs. Finally, we will discuss design strategies that have been used to integrate these QDHs into solar energy conversion devices and discuss key examples of such solar devices. The literature on optimizing and engineering various types of QD solar cell devices is already very large,[17,18,33,36,37] so we do not attempt to cover such device studies exhaustively; instead, we will focus our attention on those devices that contain well-defined QDHs, and place more emphasis on the connections between chemical synthesis, structural studies, and the fundamental physical properties of QDHs, as well as their ultimate impact on device performance.

2. Current progress in chemically synthesized QDHs

2.1 Overview of chemically synthesized nanoscale heterostructures

Significant progress in the synthesis of quantum dot nanoscale heterostructures has been made to date. In this review, we will discuss the most common methods for synthesizing semiconductor heterostructures for solar energy conversion and provide an overview of the materials combinations which have been made using those syntheses. There are three primary types of QDHs being studied today: junctions formed by proximal contact, junctions formed by molecular linkers, and linker-free epitaxial attachment, as illustrated in Fig. 2b–d in comparison with a conventional epitaxial planar heterojunction (Fig. 2a). For proximally contacted heterostructures, two materials are intercalated and physisorbed to each other, but are not chemically linked together (Fig. 2b). For linked junctions, the materials are directly connected, both chemically and electronically, *via* organic or inorganic linking molecules (Fig. 2c). For linker-free junctions, the materials are epitaxially connected, therefore they share a crystalline interface (Fig. 2d). These will be discussed in detail below together with other heterostructure synthetic methods, which include chemical bath deposition (CBD), successive ionic layer adsorption and reaction (SILAR), electrodeposition, *etc.* We will first review the preparation of the acceptor nanostructures.

2.2 Types and syntheses of acceptors in heterostructures

Acceptor materials are often high-quality, crystalline wide band gap semiconductors which are often affixed to a conductive substrate, usually fluorine-doped tin oxide (FTO) or tin-doped indium oxide (ITO) coated glass, but they can also be metal oxide nanostructures on a metal foil substrate. TiO_2 nanoparticles (NPs)

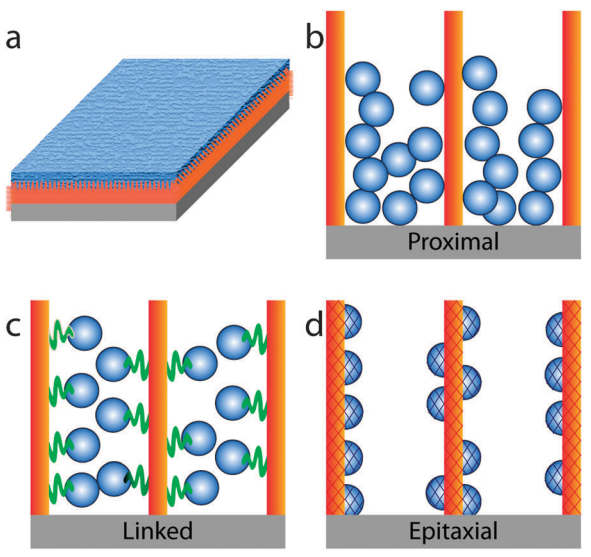

Fig. 2 Planar heterostructure (a) and quantum dot nanoscale heterostructures (QDHs) where the donor material is shown in blue and the acceptor in red. Using a QD donor and a NW acceptor as an example structure, the QDH can be (b) proximally contacted, (c) chemically-linked, or (d) epitaxial.

and various nanostructures of TiO_2[55] are the most popular acceptor oxides investigated so far. The surfaces of the as-grown acceptor materials must be treated to enable compatibility with the donor nanomaterial. Depending on the type of heterojunction desired, an organic ligand coating may need to be added or removed, the surface may need to be dehydrated, or annealing may be required to dehydrate or improve crystallinity of the surface. Commonly used methods for synthesizing wide band gap acceptor nanostructures for heterostructures include deposition of nanomaterial suspensions (*e.g.*, doctor blading or spin-casting), successive ionic layer adsorption and reaction (SILAR), hydrothermal synthesis, electrochemical etching, thermal oxidation, spray pyrolysis, and other vapor phase growth.

The simplest and most common method of creating an acceptor nanostructure for heterostructure synthesis is through deposition of as-grown nanomaterials from suspensions onto FTO- or ITO-coated glass substrates. Sol–gel grown NPs can be spin-cast or doctor-bladed onto a conductive substrate. This is the most common method to prepare the TiO_2 anode for DSSCs, and also by far the easiest method to prepare QDSSCs and QDH systems for fundamental charge transfer studies. Examples include (but are not limited to) TiO_2 NPs for use in TiO_2–CdSe(CdS)[57,68–70] and TiO_2–PbSe(PbS) QDHs,[15,16,68,71–73] SnO_2 NPs,[74–77] and Nb_2O_5 or Ta_2O_5 NPs.[15] Some of these NPs are amorphous as-synthesized, but post-synthesis heating in an autoclave increased both size and crystallinity.[15] The overall film quality can be improved by pre-treating the conductive substrate with a compact thin film of the desired metal oxide acceptor to form a blocking layer prior to applying a NP suspension. This is done by first spin-casting a solution of the metal alkoxide precursor corresponding to the wide band gap metal oxide of interest and then performing a brief low-temperature anneal.[15] SILAR allows the formation of a cohesive film on a conductive substrate. SiO_2, Al_2O_3, and ZrO_2 nanocrystalline overlayers can be created by dipping mesoporous TiO_2 NP films in organic solutions of their respective alkoxides then sintering.[78,79] Direct hydrothermal synthesis has been used to synthesize a broad range of metal oxide acceptor nanomaterials including arrays of TiO_2 NWs,[80] ZnO NWs,[51,81] SnO_2 NWs, and other oxide NWs, or hierarchical nanostructures of these oxides[82,83] onto conducting substrates. It can also be used to prepare NPs of the acceptor material to be deposited as thin films, such as in the case of sol–gel TiO_2 NPs spin-cast onto chromium-coated glass.[16]

Electrochemical etching of metal foil substrates to give vertical metal oxide nanotube (NT) arrays directly on the conducting metal foil has been a very popular method to produce metal oxide acceptor nanostructures.[84–88] The synthesis is simple and scalable; however, the resulting structures are polycrystalline. Thermal oxidation of foils or plates of several common metals—such as Fe, Cu, or W—in an (often moist) air or oxygen environment can result in the facile formation of semi-vertical metal oxide NWs on conductive metal substrates.[89,90] The growth mechanism of these NWs, however, is not fully understood. The NWs are single crystalline, but they often contain twin planes or stacking fault defects. The primary disadvantage of this thermal oxidation method of metal oxide NW synthesis is that there are typically thick metal oxide or suboxide scale layers underneath the NW array.

Spray pyrolysis is a method for creating a thin film by spraying a precursor solution on a heated substrate.[91] The temperature of the substrate is high enough to cause the precursors to react on the surface. This method can be used to deposit a polycrystalline TiO_2 thin film to improve the density and adhesion of TiO_2 NPs.[92] Acceptor nanostructures can be made using other vapor phase reactions. The extensive literature on chemical vapor deposition synthesis of NWs or other nanostructures of wide band gap oxides, such as ZnO, SnO_2, TiO_2, and, increasingly, ternary oxides,[93,94] can also be leveraged to prepare the acceptor nanostructures for QDHs. Until quite recently, solution-grown acceptor materials were only reported to be compatible with solution-grown donor materials for heterostructure formation, and likewise for furnace- and vapor-grown materials. However, this does not have to be the case, for example, one recent report outlines a method for decorating furnace-grown α-Fe_2O_3 NWs with colloidal PbSe QDs.[63]

The surfaces of these acceptor materials comprise half of a heterojunction and, consequently, the nature of these surfaces strongly influences heterostructure growth. While some surfaces are adequate as-synthesized, others require additional treatments prior to heterostructure growth or formation. For heterostructures prepared by applying a suspension of the donor material to the acceptor material, full integration of the donor material requires complete wetting of the surface of the acceptor material. Treating TiO_2 surfaces with UV light has been shown to improve wetting by suspensions in polar solvents.[95] For heterojunctions formed by purposefully linking the materials with molecular linkers, the molecules must be able to coordinate with the atoms on the surface of each material. This requires removing undesirable surface ligands and/or surface contamination, as is done for ZnO NWs: etching as-synthesized ZnO NW films with O_2 plasma prior to the introduction of suspended CdSe QDs capped with mercaptopropionic acid (MPA) has been shown to significantly increase surface coverage.[51]

2.3 Nanoscale heterojunction types and syntheses

2.3.1 Proximally contacted QDHs. In proximally contacted QDHs, sometimes referred to as ''direct attachment'' or ''direct adsorption'' heterostructures, the acceptor and donor materials are synthesized separately. The acceptor material consists of NWs or other nanostructures affixed to a substrate as a film. The donor QDs are much smaller in dimension and therefore can easily intercalate into other nanostructures. They are prepared separately using standard QD growth techniques, such as colloidal (arrested precipitation) and sol–gel syntheses, to give a suspension compatible with heterostructure formation. Then, the proximally contacted QDHs are assembled by applying a suspension of the donor QDs to the acceptor material. Methods for doing this include drop-casting (with or without doctor-blading) and spin-coating the QD dispersions.[15] Examples include PbSe QDs on vertically-oriented arrays of ZnO NWs,[50] PbS QDs mixed with TiO_2 nanobelts (as shown in Fig. 3),[96]

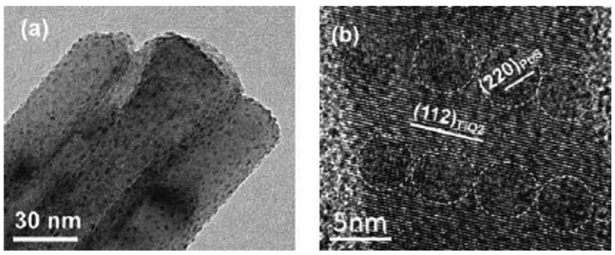

Fig. 3 An example of PbS QDs physisorbed to TiO_2 nanobelts *via* proximal contact.[96]

PbSe QDs on layer-by-layer deposited TiO_x,[97] CdS or CdSe on TiO_2[98] and ZnO,[99,100] and $CuInS_2$ QDs spin-coated onto FTO.[101] More complex semi-ordered or layered structures can be achieved through sequential applications of donor material, as in the case of a heterostructure formed by spin-casting CdSe and CdTe QDs sequentially onto alumina coated ITO.[102]

The primary advantages of proximally contacted heterostructures are low cost and facile preparation of heterostructured films over large areas. However, QDH composites made by direct attachment suffer from inhomogeneous and unordered distribution of the donor material, and the coverage of the QDs on the oxide acceptor surface is often not very high, as shown in the atomic force microscopy (AFM) images of CdSe QDs adsorbed on the single crystal TiO_2 surface (Fig. 4a).[17,103–105] More importantly, the primary disadvantage is the lack of a direct electrical connection between the acceptor and donor materials. Even though no special steps are taken to provide molecular linkers or otherwise treat the surface ligands of the donor or acceptor materials, surface capping ligands are always present on the QDs. This necessitates that charge-transfer occur *via* a hopping mechanism, resulting in an intrinsically low charge transfer efficiency in these systems. In addition, the presence of organic ligands on either or both materials further inhibits efficient electrical coupling of the QDs to the acceptor materials.[42,68,97,104–107] After the preparation, the quality of these directly deposited QD films can be improved through annealing, as in the case of CdSe QDs on TiO_2.[108,109] This could potentially remove the surfactant ligands capping the QDs (or coating the oxide nanostructures) and result in sintered nanocomposites.

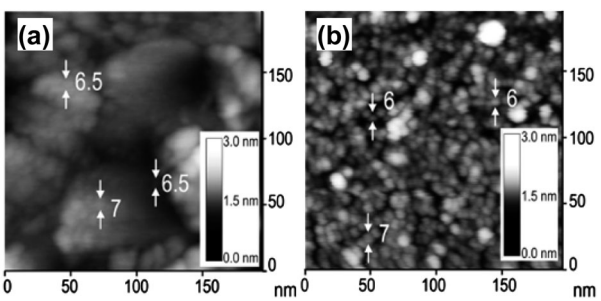

Fig. 4 Tapping-mode AFM images of rutile single crystal (a) with directly adsorbed CdSe QDs and (b) with CdSe QDs linked through MPA linkers (taken from ref. 104).

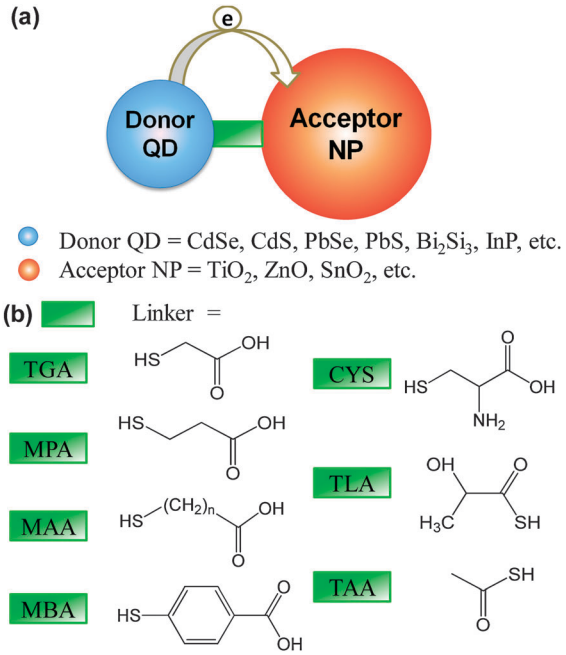

Fig. 5 (a) Schematics of QDHs connected by chemical linkers. (b) Some common examples of the chemical linkers.

2.3.2 Chemically linked QDHs. Charge transfer between acceptor and donor materials can be facilitated through an organic or inorganic molecular linker (see schematic Fig. 5a). As with proximal heterostructures, the acceptor and donor materials for these QDHs are synthesized separately. However, for chemically-linked or tethered junctions, the donor material is added to the acceptor in the presence of a bifunctional molecule exhibiting preferential binding of the different groups to the acceptor and donor materials, respectively. The thiol (–SH) group is a good ligand to bind to the surface of metal chalcogenide QDs and the carboxylic acid group (–COOH) is a good ligand to most metal oxide surface; therefore, the common choice of the bifunctional linker for QDHs are molecules that contain these two functional groups.[110] One commonly used linker is 3-mercaptopropionic acid (MPA), a bifunctional linker bearing carboxylate and thiol functional groups.[103,111,112] Several analogues of MPA with different chain lengths—generally described as mercaptoalkanoic acids (MAAs)—and aromatic (rather than alkyl chain) structures are shown in the left column of Fig. 5b. Some other commonly used linker molecules include cysteine (CYS), thiolactic acid (TLA), and thioacetic acid (TAA) (shown in the right column of Fig. 5b).[113,114] Linkers with other oxide-binding functional groups, such as phosphates, have also been explored.[73,115]

Chemically-linked QDHs have been synthesized by linking PbS, PbSe, CdSe, and CdTe QDs to a TiO_2 NP film with MPA.[51,87,107,111] MPA has also acted as a chemical linker for PbSe QDs to either TiO_2 or SnO_2 mesoporous films.[75] The first step to forming these structures is exchanging the native ligands on the donor material for the desired linking molecule. Once ligands and linking molecules are exchanged, the acceptor and donor materials are combined, and the exposed functional groups of the linking molecules attach to the acceptor material.

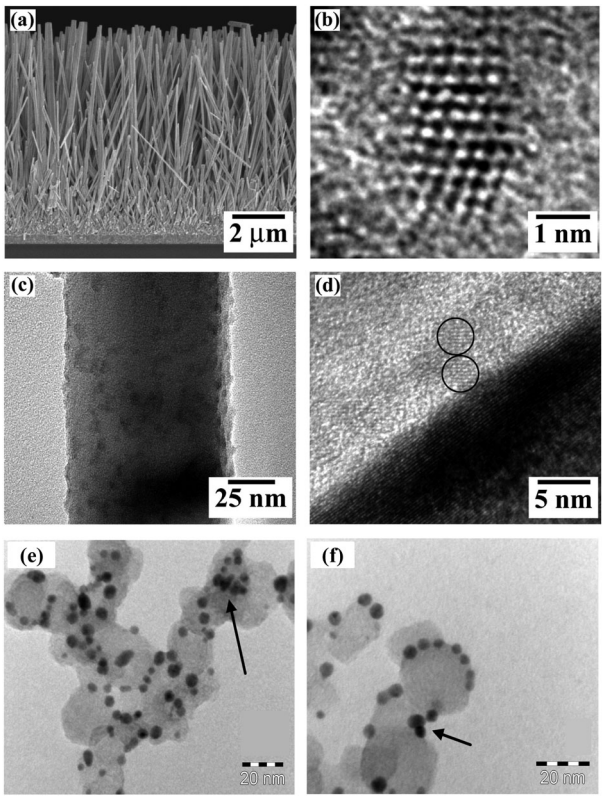

Fig. 6 Examples of QDHs connected by chemical linkers. (a–d) CdSe QDs linked to ZnO NWs *via* MPA. (a) Cross-sectional SEM of ZnO NWs; (b) HRTEM image of CdSe capped with MPA, (c, d) TEM images of CdSe QD-decorated NW (taken from ref. 51); (e, f) TEM images of PbSe QDs linked to mesoporous TiO_2 *via* MPA (taken from ref. 75).

For example, to make CdSe–ZnO heterostructures (Fig. 6a–d), the first step was to exchange the nonpolar ligands on CdSe for MPA ligands so that the thiol group of the MPA coordinated to the CdSe surface and the carboxylic acid group of the MPA was exposed. When the CdSe QDs were introduced to the ZnO NWs, the COO^- group coordinated to the ZnO surface, linking the heterostructure.[51] The reverse order of operation, *i.e.* attaching the linker molecules to the oxide acceptor nanomaterials first followed by binding to donor QDs, is also commonly employed, as seen in the example of PbSe QDs linked to TiO_2 NPs by MPA (Fig. 6e and f).

Chemically-linked heterostructures can also be formed concurrently with synthesis of the donor nanomaterial. Bi_2S_3 QDs were synthesized from BiI_3 and H_2S in the presence of a TiO_2 NP substrate and MPA *in situ* in one solution reaction. This resulted in Bi_2S_3 being linked to TiO_2 by MPA during QD growth.[92] In another one-step CBD of the donor materials to form QDHs, CdTe or CdTe/CdS QDs were linked to TiO_2 NPs with a thioglycolic acid (TGA) bifunctional linker, which also serves as a stabilizer and precursor sulfur source.[116] Chemical linker strategy and proximal contact strategy can be applied to the same QDH system. For example, submerging a TiO_2 film in a suspension of InP QDs coated with short chain phosphine ligands resulted in adsorption of the QDs onto the TiO_2, forming the proximally contacted structure. The InP NCs could also be molecularly linked to the TiO_2 NPs with thiolactic acid (TLA, see Fig. 5b).[117] The details of various linking strategies have been thoroughly reviewed in a recent Perspective.[103]

In comparison to proximally contacted QDHs, the use of purposefully designed linker molecules can increase the surface coverage of QD donors and improve the electronic communication across the QDHs. Replacing the surface capping ligands on the donor QDs with bifunctional linkers that coordinate to the acceptor nanostructures has been shown to suppress the aggregation of QDs[104,105,112] and increase the surface coverage (see Fig. 4b), spatial consistency, and experimental reproducibility of QDs adsorbed on nanocrystalline TiO_2 films.[104,112] More importantly, the rate and mechanism of the electron transfer in QDHs will depend on the linker molecule. While linker molecules such as MPA alter the electronic structure at the interface and, hence, the electron transfer rate, the electron energy alignment between the acceptor and donor materials will not be affected. Kamat and co-workers investigated the effects of chain length on chemically-linked CdSe–TiO_2 QDHs using three bifunctional molecules composed of a carboxylate functional group linked to a thiol functional group by a carbon chain of varying lengths: thioacetic acid (TAA), MPA, and mercaptohexadecanoic acid (MDA).[111] More systematic studies of various analogues of MPA linkers carried out by Watson and others have clearly shown that shorter chain linkers promote electron transfer.[103] The impact of these details on charge transfer has been carefully investigated and will be discussed in Section 4. Despite the advantages of chemically-linked nanostructures, the lack of a direct lattice connection could still pose a barrier to efficient charge-transfer. Indeed, without a resonant charge-transfer mechanism or conjugation within the linker, electron transfer occurs *via* tunneling, and the transfer rate decreases with increased linker size.[103]

2.3.3 Epitaxially grown QDHs. The most efficient configuration for charge-transfer across heterojunctions is through high-quality epitaxial interfaces. Unlike proximal or chemically linked QDHs, epitaxy promotes direct electronic communication between the donor and acceptor. While epitaxial interfaces are the most technically challenging to achieve among the heterostructures discussed, such heteroepitaxy is more likely to be achieved for nanoscale heterostructures. As discussed in Section 1.3, the nanoscale dimension can better tolerate interfaces formed between crystal lattices with large lattice mismatches and different crystal structures than their bulk counterparts.[58,59,61] To form a high-quality epitaxial connection, the two-dimensional (2D) translational symmetry of the crystal lattice of the donor and accepter materials at their shared interface must share a relatively small, lattice-matched supercell.[58] On the scale of nanometers, this requirement can be commonly met, resulting in apparently fortuitous heteroepitaxy.[8]

Compared with the two previous types of QDHs, reports of definitive epitaxial QDHs have been much less common. There are two synthetic routes for epitaxial heterostructures: the one-pot synthesis of a QDH suspension which is subsequently deposited on a conductive substrate, and the direct growth of a donor material on an acceptor material attached to a conductive substrate. An example of a one-pot reaction is the epitaxial

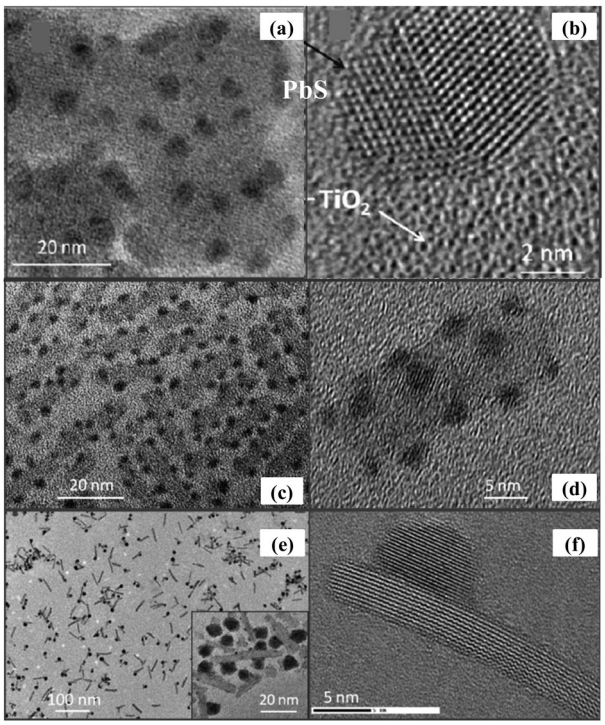

Fig. 7 Examples of epitaxially linked QDHs. PbS QDs on mesoporous TiO_2 and TiO_2 NRs (taken from ref. 68 and 118).

growth of PbS QDs on the surface of suspended colloidal TiO_2 nanorods (NRs) reported by Zamkov and co-workers, as shown in Fig. 7c–f.[118,119] Once synthesized, these materials were drop-cast onto a transparent conducting oxide substrate.

An example of the sequential synthesis of the donor nanomaterials onto a substrate-bound acceptor is the case of a drop-cast TiO_2 NP film on ITO which was placed in the reaction vessel where high temperature QD (PbS, PbSe, and PbTe) precursors were injected, resulting in their heterogeneous nucleation and growth on the TiO_2 NPs, as shown in Fig. 7a and b.[68] The lattice connection was likely epitaxial, though the TEM characterization was inconclusive. The CdS decorated TiO_2 film can be further converted to Cu_2S *via* standard NC ion exchange syntheses.[68] For these examples above, although there is a direct connection between the donor and acceptor materials, there is no direct electrical connection between the acceptor and an electrically conductive substrate.

In contrast to the heterostructures discussed above, QDHs have also been synthesized using direct colloidal growth on acceptor nanostructures directly connected to conducting substrates. Epitaxial heterostructures of PbSe QDs on α-Fe_2O_3 NWs prepared by thermal oxidation,[63] which are directly attached to a conductive steel substrate, have been successfully synthesized by combining the colloidal QD synthesis with the as-synthesized NWs (Fig. 8A). The key to this QDH formation is a vacuum surface treatment that we have developed to remove the surface adsorbed water that is almost always present on the surface of iron oxide and other metal oxides.[120] The direct heterogeneous nucleation of PbSe QDs on α-Fe_2O_3 NWs relies upon an aggressive surface dehydration of the as-synthesized α-Fe_2O_3 NWs at 350 °C under vacuum (about 20 mTorr) followed by the introduction of PbSe QD colloidal precursors. This procedure results in the direct epitaxial growth of PbSe on the surface of the α-Fe_2O_3 NWs. Additionally, this synthesis is tunable: the density of QDs on the NWs and QD diameter distribution increases with the duration of the dehydration, and a lower injection temperature of the QD synthesis reagents results in QDs with smaller diameters and narrower size distributions. Detailed TEM structural analysis (Fig. 8B–E) reveals an example of direct heteroepitaxial QDHs, where the matching crystal faces are the PbSe (002) and α-Fe_2O_3 (003) with their respective [1$\bar{1}$0] crystallographic directions aligned, as illustrated in Fig. 8F and G. This example demonstrates that fortuitous heteroepitaxy can occur readily in nanoscale heterostructures in general. In addition to the heteroepitaxy and the direct electrical pathway through NWs to conductive substrates, this is the first report of heterostructures synthesized combining both colloidal and vapor phase methods. Instead of using the high vacuum and high temperature growth of QDs, this method uses colloidal solution growth aided by a simple dehydration step. This strategy can allow a broad range of acceptor nanomaterials made by diverse synthesis routes[55,93,94,121] to be integrated with QDs to create the high-quality, epitaxial nanoscale heterostructures that can be useful for fundamental solar investigation and practical applications.

2.4 Other synthetic strategies for heterostructures

Other synthetic strategies that have been employed to create QDHs include CBD, SILAR, electrodeposition, and other one-step vapor synthesis methods. These methods generally provide less control over the QD size, dispersity, and morphology than the methods discussed above, but they are usually quite simple and scalable; therefore, they are very popular for preparing QDSSCs. In the frameworks of the QDH types classified above, these methods result in QDHs without intentional ligands or linkers, providing the potential to form epitaxial QDHs. In fact, some of these methods may have the potential to grow, or may have already grown, heteroepitaxial structures, but most of the reports did not contain the detailed microstructural analysis necessary to confirm epitaxy.

CBD is performed by submerging a substrate in a dilute solution of the precursors required for the synthesis of the donor material. At proper concentrations, the donor material is deposited on the acceptor film and also precipitates from solution.[122] CBD is a straightforward technique which has no restrictions for acceptor material, dimensions or morphology and which can be easily modified for a broad range of donor and acceptor materials, such as CdSe/CdS on TiO_2[86,123–129] and CdS QDs on ZnO NWs.[130–133] In addition, it does not require vacuum or high temperatures. The disadvantages of CBD are the extended time required and the difficulty in controlling results. Other alternative forms of CBD include microwave-assisted chemical bath deposition (MACBD) (as shown in the example of CdS synthesis on TiO_2[134]), sonication-assisted sequential

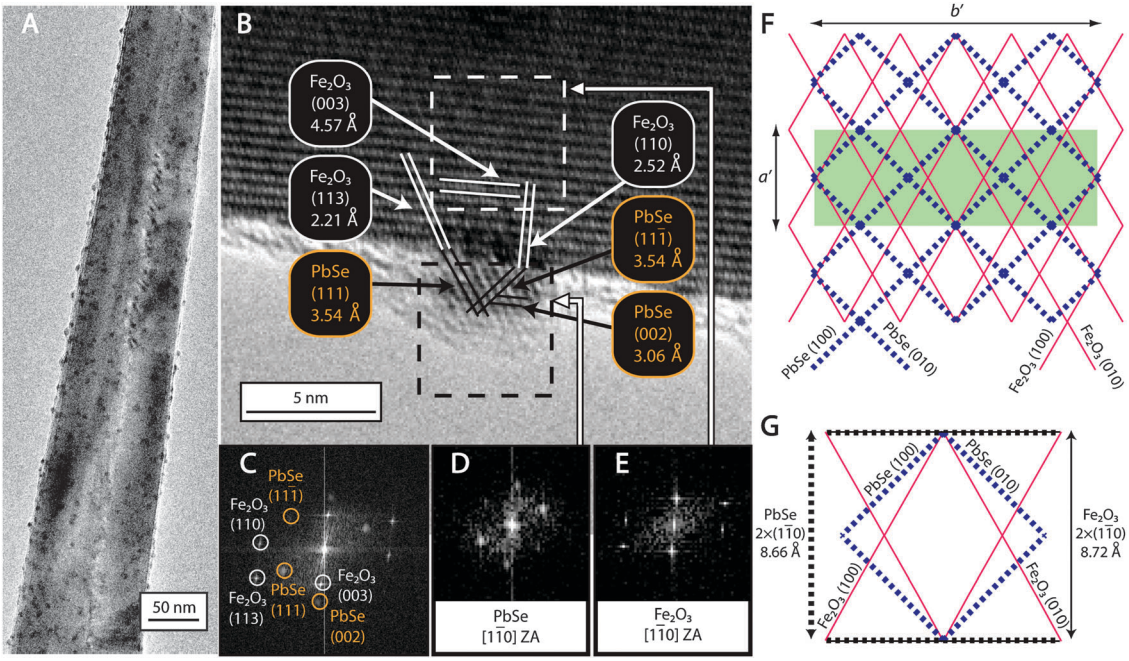

Fig. 8 An example of epitaxially linked QDHs. PbSe QDs were directly grown colloidally on Fe_2O_3 NWs that have been prepared in high temperature reactions (taken from ref. 63).

chemical bath deposition (S-CBD) (as shown in the example of CdS QDs on TiO_2 NT arrays),[135] and SILAR.

SILAR is a more refined version of CBD that has been successfully employed to synthesize many heterostructures with metal chalcogenide donor materials.[15,122] These structures are formed by successively dipping a substrate bearing the acceptor material into a solution with metal cations, followed by dipping in a solution containing a chalcogenide precursor. The size of the donor material can be increased by repeating the coating procedure.[16] The primary benefit of SILAR over conventional CBD is that the size of the QDs can be controlled to some degree by the number of SILAR reaction cycles. Another advantage is that for porous acceptor materials, SILAR provides a method to grow QDs inside pores through which the QDs could not physically pass. Disadvantages of this method include a large QD size distribution, inferior QD stability, and a lack of control over QD morphology.[68,122,136] The TEM images of some examples of QDHs made by SILAR (Fig. 9a and b) clearly show these points. This method has been used to form heterostructures of PbS, CdS, Ag_2S, Sb_2S_3, or Bi_2S_3 on TiO_2, Nb_2O_5, Ta_2O_5, SnO_2, or ZnO NP films,[15] and have been commonly used to make the heterostructures of CdS, CdSe, PbS on nanocrystalline oxides for QDSSCs.[17,18,38,77,81,137–143] Other more diverse donor materials prepared through SILAR include $CuInSe_2$[144] and $CuInS_2$ on TiO_2 nanotube arrays,[133] $In(OH)_xS_y$/$Pb(OH)_xS_y$ on SnO_2,[145] and CdS on SnS.[146]

Electrodeposition is also a commonly reported method for the preparation of nanoscale heterostructures. A substrate is suspended as an electrode in a precursor solution and current passed through the substrate results in reduction (or oxidation) of the precursors at the electrode surface, resulting in nanomaterial growth.[70]

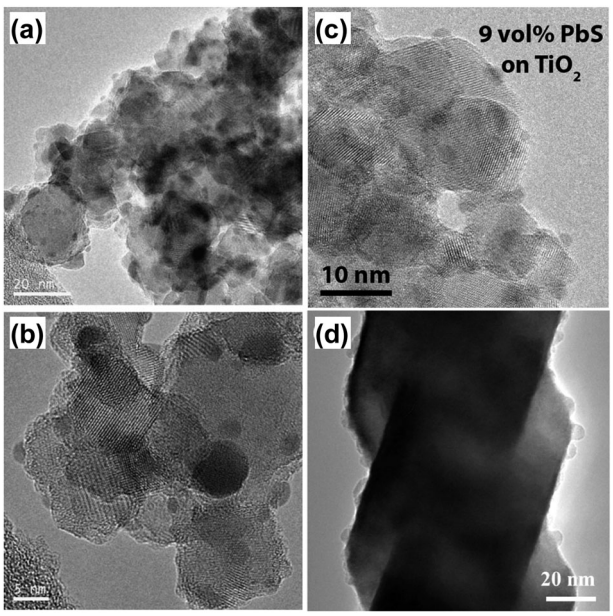

Fig. 9 Examples of (a, b) PbS QD on TiO_2 NP films made by SILAR (taken from ref. 38), (c) PbS QD on TiO_2 NP films made by reducing flame spray pyrolysis (taken from ref. 147), and (d) CdSe QDs on Zn_2SnO_4 NWs synthesized using pulsed laser deposition (taken from ref. 148).

The benefits of electrodeposition include the ability to form heterostructures with precise control and the ability to coat large, irregular areas with varying topologies. Unfortunately, these materials often suffer from impurity phases and low morphological quality.[149] Examples include the electrodeposition of $Cu(In,Ga)Se_2$ on CdS NWs,[150] CdSe QDs on TiO_2 nanostructures,[80,151]

CdS nanostructures on TiO_2 NTs,[152–154] and CdTe on ZnO NW arrays,[155] and a multilayered heterostructure consisting of patterned p-Si nanopillars coated with a layer of electrodeposited CdSe QDs then a layer of a ZnO film using CVD, and finally ZnO NWs.[156] Likely epitaxial QDHs can be made by sublimation[88] and chemical vapor transport or deposition of the donor nanomaterials[157] onto acceptor nanostructures on conducting substrates. Epitaxial QDHs can also be made through an entirely vapor phase synthetic route, such as the atomic layer deposition (ALD) deposition of chalcogenide QDs,[158] PbS QD deposition on TiO_2 nanoparticles *via* reducing flame spray pyrolysis (Fig. 9c),[147] and CdSe QDs deposition on Zn_2SnO_4 NWs using pulsed laser deposition (PLD) (Fig. 9d).[148]

3. Structural characterization of QDHs

The properties of the heterostructures depend on the details of the nanostructures and microstructures. Standard materials characterization techniques are employed to determine the morphology and crystallinity of both the separate donor and acceptor components and their shared interface. The morphology of the individual QDH components and of the complete QDH itself can be evaluated through scanning electron microscopy (SEM). Very small donor materials and fine details must be studied using transmission electron microscopy (TEM) and high-resolution transmission electron microscopy (HRTEM), which allow for the evaluation of the crystallinity of the components and their shared interface. In the case of an epitaxial QDH, orienting the sample such that both the acceptor and donor materials are on zone axes elucidates the orientations of the components with respect to one another and allows direct visualization of the crystallographic plane alignment at the interface, as shown in Fig. 8.[63] Using these data, the epitaxial supercell and lattice mismatch percentages can be calculated. Elemental mapping can be performed using a scanning transmission electron microscope (STEM) equipped with an electron dispersive spectroscopy (EDS) or electron energy loss spectroscopy (EELS) detector, which provides confirmation of the elemental composition of the acceptor and donor materials and the distribution of different phases. While TEM and SEM can be used to evaluate the individual components and heterojunctions, ensemble characterization is also required, as most QDHs are prepared and used as ensembles. To confirm the crystallinity and purity of the donor and acceptor materials, QDHs can be evaluated by X-ray diffraction (XRD).

Due to their large surface area-to-volume ratio, understanding the surface composition of QDHs is important to the overall function. Surface characterization techniques, including Fourier transform infrared spectroscopy (FTIR) and X-ray photoelectron spectroscopy (XPS), allow determination of the original ligands, confirmation of effective exchange of ligands, and the attachment of chemical linkers, if present.

4. Charge transfer in QDHs

Charge separation and transfer is a critical step in the solar energy conversion process. While solar materials must be capable of absorbing sunlight to create charge carriers, without charge separation, the carriers can readily recombine, so that they can be neither collected nor used for catalysis (in the case of PEC). Absorption and photoexcitation generally occurs primarily in the donor material, but may also occur in the acceptor. Efficiently harvesting solar energy requires two materials, at least one of which strongly absorbs light over the full range of the solar spectrum, and the valence and conduction band energy alignments of the donor and acceptor materials must facilitate charge separation at their interface. This fundamental principle holds true for QDHs.

4.1 Design and band alignment of heterostructures

From the conventional perspective, charge transfer across the heterojunction is driven by the electronic band structure alignment of the acceptor and donor materials. There are three types of band gap alignments: straddling (type I), staggered (type II), and broken (or misaligned, type III) (Fig. 10). For type I heterostructures, both the hole and electron accumulate in one of the two components. This does not promote the flow of charge carriers required for solar energy conversion; instead, this band alignment promotes recombination. The hole and electron are separated into different components for type II and type III heterostructures and are the desired band alignment for charge separation. When designing bulk heterostructures for solar energy conversion, materials choices and combinations are limited, as the band gaps and band energy levels[159] that define the band alignment are material specific. This requirement is relaxed for QDs, whose band gaps and band positions are tunable by size due to quantum confinement.[40,41] Energy band alignments for QDHs can be estimated for a pair of nanomaterials through calculations and modeling, and the band positions of each component—bulk or quantum confined—can also be experimentally measured.[160,161]

4.2 Mechanisms of charge transfer in QDHs

The driving force for separating charge carriers is only one of the important characteristics: the mechanism and, thus, the efficiency and rate of the charge transfer are also significant. Charge separation can occur in all types of QDHs described in this review—proximally contacted, chemically linked, and epitaxial—albeit by

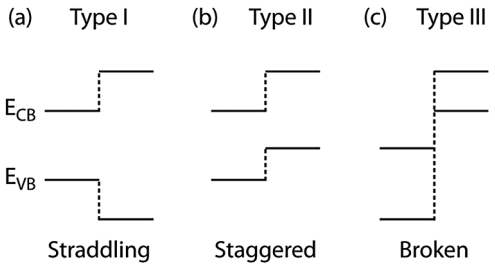

Fig. 10 Various heterostructure band alignments. (a) For type I heterostructures, the band energy levels of one material straddle those of the other, resulting in the transfer of both holes and electrons to the narrower band gap material; (b, c) for type II and III heterostructures, the band energy levels are staggered or broken, respectively, so that charge separation is energetically favorable.

different mechanisms and with different efficiencies. There are three primary types of charge-transfer: quantum mechanical tunneling, where phase coherence is preserved during the transfer; tunneling between multiple potential wells, where coherence is lost in each well (when the charge resides in the potential well); and thermally activated incoherent hopping without phase coherence.[3] Many efficient solar energy conversion systems display characteristics of coherent charge-transfer.[31,162–171] Recent developments in DSSCs[13] and QDSSCs[9,18,166] show that the most efficient charge separation and transport dynamics involve the time evolution of wave functions. There is evidence that natural photosynthetic systems appear to have evolved complex nanostructures that retain the quantum mechanical phase coherence during the primary photosynthetic charge separation event.[163–165] The DSSC's charge separation also appears to involve non-classical femtosecond coherent transport.[172] This process may involve superexchange—coherent quantum tunneling through molecular orbitals that are different from the donor and acceptor. For coherent tunneling, there is an exponential dependence of rate on separation distance.

Therefore, charge separation is most efficient when the heterostructure design creates proper band energy alignment at high-quality, epitaxial interfaces. For non-epitaxial materials, careful tuning of the band alignment and, hence, the driving force for charge separation can increase the transfer rate; when the energy gap of the heterojunction is zero, tunneling is not distance dependent.[3] For proximally contacted or chemically linked QDHs, charge transfer can occur *via* coherent tunneling or diffusive or incoherent hopping. Tunneling is a fast process where the charge carrier never resides on the linking molecule during charge transfer. In contrast, incoherent hopping in the same structures is a much slower process in which the charge carrier resides on the linking molecule during charge transfer. For the diffusive hopping mechanism, charge transfer is inversely proportional to the length of the linker or distance between the components.[3,103,115,173] In addition to these mechanisms, transfer can occur in chemically linked QDHs through thermally activated or non-activated reduction or oxidation of the linking molecule. The charge may reside on or be delocalized over the linker when the charges are transferred across the heterojunction.[3]

4.3 Investigation of charge transfer in QDHs

The most common techniques for investigating charge transfer across QDHs are steady-state and time-resolved optical spectroscopy. In these experiments, photoexcitation creates an electron–hole pair and their dynamics are measured. The electron transfer between CdSe, CdS, PbS, or PbSe QD donors to a TiO_2 acceptor (NPs or other morphologies) with proximal contact or molecular linkers has been extensively investigated[31,57,74,76,103,107,111,115,166,173–176] and some prominent features will be discussed below, both as an illustration of the techniques that can be used to investigate the charge transfer and also to emphasize the key points in designing such QDHs. In contrast, the examples of epitaxial QDHs are less common, and their charge transfer properties have not been investigated in depth.[118,119] There has been preliminary investigation of charge transfer dynamics in QDHs prepared by SILAR and other methods that yield QDHs with a direct connection rather than proximal or molecularly linked contact.[140,177,178]

Standard absorption/emission spectroscopy is an example of steady-state spectroscopy. For unbound CdS QDs illuminated with 480 nm light, a strong emission was observed at a longer wavelength (QD size dependent). When CdS QDs are attached to TiO_2 NPs using a series mercaptoalkanoic acid (MAA) linkers of varying lengths (see Fig. 5b), the emission from CdS is greatly reduced, as shown in Fig. 11a.[103,173] This change confirms the deactivation of the excited CdS by electron transfer to the TiO_2 NPs.[42,99,173]

The most common time-resolved studies are carried out by illuminating the QDH at a specific wavelength and following the responses in transient absorption (TA) or transient

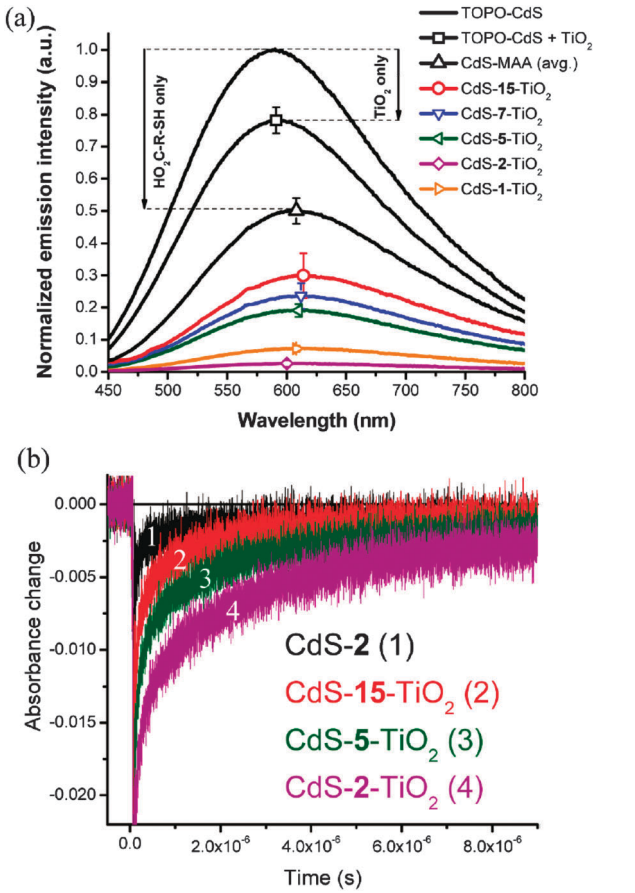

Fig. 11 Examples of steady-state and time-resolved spectroscopy of chemically linked QDHs. (a) Normalized emission spectra for TOPO-capped CdS QDs, mixtures of TOPO-capped CdS QDs and TiO_2 NPs, mixtures of TOPO-capped CdS QDs and MAAs (averaged for several chain lengths), and CdS–MAA–TiO_2 QDHs (the bold number equals the number of CH_2 groups of the MAA). Emission quenching for CdS-15-TiO_2 corresponds to additive quenching from TiO_2 and the linker alone; for shorter linkers, electron injection gives rise to additional quenching. (b) Decay of the 480 nm bleach of MPA-functionalized CdS QDs and CdS–MAA–TiO_2 QDHs following pulsed excitation at 415 nm. The amplitude and lifetime of the bleach decrease with increasing length of the MAA linker (taken from ref. 103).

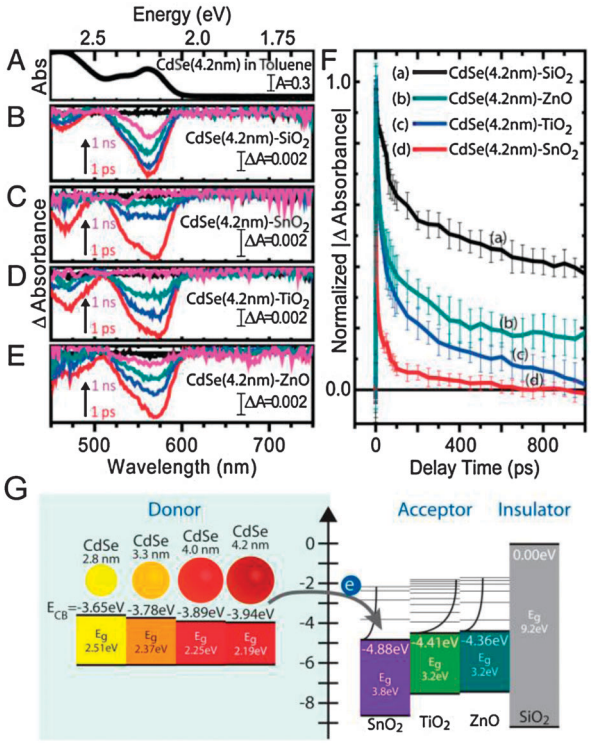

Fig. 12 Examples of the time-resolved spectroscopic investigation of chemically linked QDHs. (A) UV-visible and (B–E) transient absorption spectral traces of 4.2 nm-diameter CdSe QDs in (A) toluene and attached to (B) SiO_2, (C) SnO_2, (D) TiO_2, and (E) ZnO. Trace colors indicate transient spectra at pump–probe delay times of 0 (black), 1 (red), 10 (blue), 100 (cyan), and 1000 ps (pink). (F) Transient absorption kinetic traces of 4.2 nm-diameter CdSe QDs attached to each metal oxide substrate at the $1S_{3/2}$–$1S_e$ transition. (G) Diagram of the relative electronic energy differences between CdSe QD donors and metal oxide acceptors. Taken from ref. 74.

photoluminescence (PL). Time-resolved spectroscopy provides confirmation of charge transfer and a mechanism for determining the rate at which the transfer occurs (k_{ET}). Some examples carried out on chemically linked QDHs are shown in the transient absorption spectra with different pump–probe time delays in Fig. 12A–E and the kinetic traces of the transient absorption are shown in Fig. 11b and Fig. 12F. They will be discussed in the context of the specific QDH samples below.

The charge transfer in molecularly linked (or tethered) QDHs of CdS and CdSe QD donors and TiO_2 and other common metal oxide acceptors has been investigated and understood in detail.[57,74,103,173–175] The charge transfer rate and mechanisms in these QDHs are influenced by the driving force from the band energy alignment, the linker length, and the electronic coupling. Kamat and co-workers showed that the band gap and band energy levels of the donor QDs are tunable through the physical QD size.[57] In addition, different metal oxide acceptors have different band gaps and band positions. The combination of these two factors allows for different band energy alignments and varying driving forces for the charge transfer from the donor QDs to the acceptor oxides (Fig. 12G).[74] Transient absorption spectra for 4.2 nm diameter CdSe QDs on various metal oxide acceptors following 387 nm excitation at different pump–probe delay times (Fig. 12B–E) show different rates of suppression due to electron injection from the CdSe QDs to the metal oxides. This difference can be more clearly compared in the transient absorption kinetic spectra (Fig. 12F). These kinetic traces can be fitted to a bi-exponential (or multi-exponential) decay functions to yield lifetimes (τ) or convoluted lifetimes of various physical processes. From these, the ultrafast electron transfer rates (k_{ET}) can be estimated. The ultrafast electron transfer time is generally in the picosecond range, and the electron transfer rates are typically in the range of 10^7 s^{-1} to 10^{11} s^{-1}, depending on the driving force. These differences demonstrate that the dynamics and efficiency of the charge transfer between these QDHs can be controlled by the different driving forces. The variation of the electron transfer rate with the estimated driving force can be modeled by semi-classical Marcus theory in the QDH systems.[74] The similar finding that small PbS QDs are needed to enable suitable band energy alignment and driving force has been made in the PbS–TiO_2[107] and PbS–SnO_2[76] QDH systems by other researchers, but the observed time scale of the electron transfer (100 ns) was slow.[107] Watson and co-workers systematically investigated the kinetics and efficiency of charge transfer between CdS QDs and TiO_2 NPs chemically linked by a series of MAA linkers with varying chain lengths (see Fig. 5b). As shown in Fig. 11a, the emission of the CdS QDs is progressively quenched as the chain length of the MAA linkers becomes shorter. This dynamic emission quenching is attributed to the injection of electrons from the CdS QDs to the TiO_2 NPs, as discussed above. The long-lived bleach of a broad ground-state absorption band seen in Fig. 11b is associated with the charge-separated state. The clear dependence of the emission quenching and the duration of this bleach on the chain length of the MAA linker shows that the high electron transfer rate and yield occur for shorter molecular linkers. Hyun *et al.* employed time-resolved fluorescence techniques in the chemically linked QDHs of PbS QDs on TiO_2 NPs to investigate the variation of electronic coupling between the PbS QDs and the TiO_2 NPs by changing the length, aliphaticity and aromaticity, and anchor groups of more chemically diverse linker molecules, and sought to understand this coupling within the framework of Marcus theory.[115] Again they found that shorter linker molecules consistently lead to faster electron transfer. The electron transfer rate can vary dramatically with different anchor groups, but is not sensitive to the distinct aliphatic or aromatic character of the linker molecule. There is also preliminary work showing that charge transfer in CdSe–TiO_2 QDHs prepared by SILAR is generally faster than in analogous QDHs with molecular linkers.[140]

There are fewer systematic spectroscopic studies in linked lead salt QDHs on TiO_2 or other oxide acceptors,[76,179] but the basic situation can be analogous to that for CdS and CdSe. Hyun *et al.* reported the time scale of electron transfer for PbS QDs linked to TiO_2 NP to be in the relatively slow nanosecond range,[107,115] as did Bonn and co-workers for PbSe QDs on TiO_2 NP films.[75] However, Lian and co-workers observed the ultrafast electron transfer time of 6.4 ± 0.4 fs for PbS QDs linked to TiO_2 NP films with MPA,[176] which is argued to be conducive for

extracting photoexcited carriers from potential hot electron transfer or MEG processes. Ultrafast electron injection (estimated to be <50 fs) from PbSe QDs to single crystal TiO_2 and hot electron transfer was observed by time-resolved surface harmonic generation (SHG) spectroscopy by Zhu and co-workers.[31] It is not yet clear what causes the discrepancy in these reported electron time scales of ns *vs.* fs.

4.4 Emerging techniques for investigating charge transfer in QDHs

Multiresonant coherent multidimensional spectroscopy (CMDS) is emerging as a very powerful method for probing the coupling between the quantum states of nanostructures as well as their dynamics.[180,181] It is a methodology that is quite different yet still related to the traditional pump–probe and transient absorption ultrafast spectroscopic methods. To perform CMDS, multiple tunable femtosecond or picosecond excitation pulses are focused into a sample, resulting in the formation of multiple quantum coherences (MQCs) of the quantum states within a heterostructure. MQCs are quantum mechanical superposition states formed by exciting multiple quantum states within the time period during which they retain the phase of their quantum mechanical wavefunctions. The temporal oscillations of pairs of quantum states emit new electromagnetic fields. Since the oscillations have well-defined phases throughout the excitation volume, the emission is cooperative, intense, and directional. The emission is enhanced by resonances with the quantum states so that scanning the pulse frequencies creates multidimensional spectra and scanning the time delays between excitation pulses measures the coherent and incoherent dynamics. Multiresonant CMDS has a much higher resolution and larger dynamic range than standard ultrafast methods because the multiple transitions multiplicatively enhance the emission if they occur on the same QD.

Picosecond CMDS has been successfully used to reveal quantum state resolved dynamics of the intrinsic electronic states[182,183] as well as surface states in PbSe QDs.[184] Fig. 13 shows some examples of these experiments, in which two excitation pulses having a frequency ω_2 excite the 1S quantum state and a third excitation pulse having a frequency ω_1 arrives 2 ps later and causes the 1S state population to undergo transitions to the ground state or a biexcitonic state. Fig. 13a shows how the output intensity depends on ω_1 and ω_2. The diagonal character results from line-narrowing. It occurs because the ω_2 excitation is resonant with PbSe QDs with a particular size within the inhomogeneous ensemble of QDs. The ω_1 excitation frequency then provides a second resonance enhancement for the particular QDs excited by ω_2. When ω_2 changes, the ω_1 frequency also changes as different size QDs become doubly resonant. The length along the diagonal measures the inhomogeneous broadening and the width across the anti-diagonal measures the homogeneous broadening. Fig. 13b shows an example of how this methodology is sensitive to the dynamics of forming surface states. The spectrum changed dramatically as this particular QD sample degraded over a month. Although the ω_2 pulse still excited the 1S state, the ω_1 resonance was shifted by $\sim$600 cm^{-1} because the 1S state underwent ultrafast relaxation to a surface state that lay 600 cm^{-1} lower in energy.

CMDS can also examine the dynamics of particular features in the 2D spectrum. Fig. 13c (data) and 13d (simulation) show

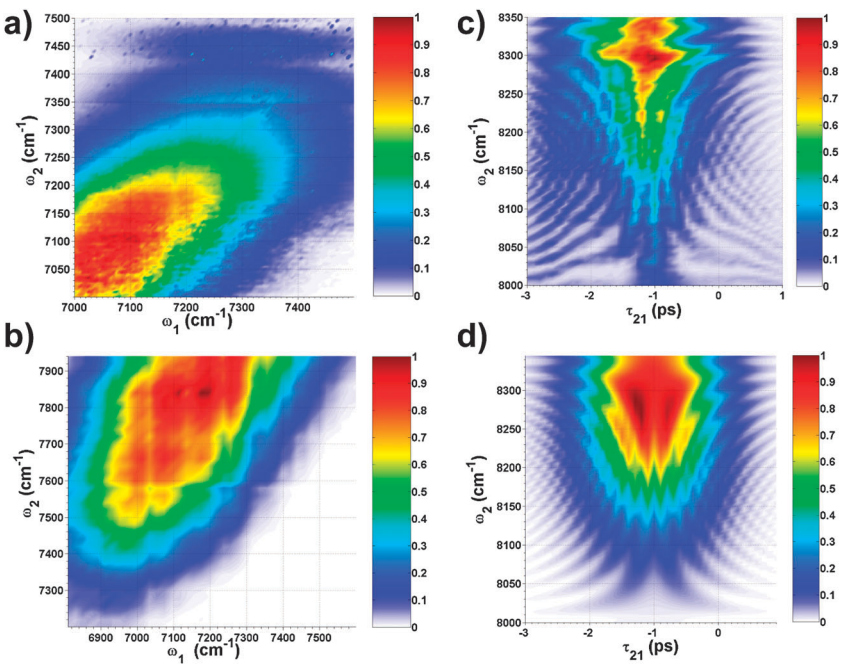

Fig. 13 The dependence of CMDS intensity in PbSe QDs on excitation frequency and time delay. The color bar indicates output intensity. (a) The dependence on the two excitation frequencies for a typical PbSe QD; (b) dependence on two excitation frequencies for an aged PbSe QD sample; (c) dependence on the ω_2 excitation frequency and the time delay between the last excitation pulse and the first two pulses; (d) a simulation of the data in (c). Taken from ref. 182 and 184.

the intensity dependence on ω_2 and the time delay between the ω_2 pulses and the ω_1 pulse. The intensity changes occurring on the picosecond time scale measure the decay of the 1S population while the changes occurring on the sub-picosecond time scale measure the rapid phase oscillations of the coherence between the 1S and ground state.

These preliminary experiments demonstrated the feasibility of CMDS for studying QDs and extracting the dephasing rates, the inhomogeneous broadening, the Coulombic coupling within the biexciton, and the relative transition probabilities for the excitonic and biexcitonic transitions. However, shorter excitation pulses are necessary to take full advantage of the CMDS methods. CMDS uses 16 pathways for creating the coherences and/or populations, which differ in the time orderings and resonances for the three excitation pulses. Each pathway has advantages for defining specific features in the dynamics and spectroscopy. It is possible to isolate individual pathways by imposing a specific time ordering on the excitation pulses and spectrally resolving the output frequency. It is then possible to get the complete coherent and incoherent dynamics with single quantum state resolution. Since coherent dynamics and electron transfer often occurs on femtosecond time scales in the QDHs for solar applications, it is important to use femtosecond excitation pulses. Such femtosecond CMDS techniques can be applied in the future to investigate (coherent) charge transfer in QDHs to fully probe changes in individual quantum states and their coherent and incoherent dynamics over all time scales from carrier creation, carrier recombination, and charge transfer.

Solar energy conversion using QDH requires separating charge carriers under solar illumination. Surface photovoltage (SPV) is a contactless technique for characterizing semiconductors by observing changes in surface voltage resulting from illumination at a given wavelength.[185] SPV measurements can also confirm the occurrence of charge separation and provide information about the charge carriers and their dynamics: the identity of the dominant carrier, lifetime, and diffusion length.[131,186–188] When the contact to the nanomaterial is an atomic force microscope (AFM) tip, the charge separation on individual nanostructures can be measured with spatial resolution.[189,190]

There are other valuable techniques for studying charge transfer in QDHs. When charge transfer from QDs to an acceptor occurs, charges can build up on the surface of the acceptor, which can be probed using non-linear spectroscopic techniques such as surface harmonic generation (SHG) spectroscopy.[31] Using time-resolved SHG, hot-electron transfer from PbSe QDs to TiO_2 was convincingly demonstrated and followed in real time.[31] Single-molecule spectroscopy (SMS) with near-field optical scanning microscopy can observe charge transfer between single adsorbed molecules on semiconductor surfaces or single QD and QDH.[3,191]

5. Solar energy conversion devices based on QDHs

For any solar energy conversion device based on a QDH, the QDH itself is the key component, fulfilling the functions of both light absorption (photoexcitation) and charge carrier separation. However, to realize complete light-to-electricity (PV) or light-to-chemical fuel (PEC) energy conversion, the QDHs must be integrated with other components, such as electrodes; a hole-transporting material, such as an electrolyte solution containing a chemically and energetically compatible redox couple (for liquid-junction devices),[6,17,18] a conducting polymer (either as a polymer hole-transporting material or for a general hybrid inorganic–organic device[33]), or another inorganic material that can make conformal contact with the QDs and accept and transport holes;[192] and possibly catalysts (for PEC devices). In addition, material compatibility should be considered to ensure that the devices are stable over time, *i.e.*, not degraded through regular operation by photocorrosion[17,18] or chemical instability.

In general, the efficiency of a PV device is described by its open-circuit voltage (V_{oc}), short-circuit photocurrent density (J_{sc}), and the fill factor (FF), which expresses the ratio of the maximum output power density of the device to the product of V_{oc} and J_{sc}. The overall conversion efficiency of the device is given by dividing the product of these three key parameters by the power density of the incident illumination. Standardized measurement of the overall solar conversion efficiency requires solar device characterization under light spectrally matched to that of the sun. The quantum efficiency (QE), or incident photon-to-electron conversion efficiency (IPCE), of a solar device is the wavelength-dependent ratio of the number of collected charge carriers to the number of incident photons. This is determined by measuring the current produced by a solar energy device incorporating QDHs at various wavelengths of known intensity. Quantifying the fraction of incident light that is absorbed by the device (as opposed to transmitted or reflected) allows computation of the absorbed photon-to-electron conversion efficiency (APCE), which better characterizes the efficiency of charge carrier separation within the device. These various modes of PV characterization apply directly to solar devices incorporating QDHs.

5.1 Principal design types of QD-based PV devices

Most QD-based PV devices can be categorized into three principal types based on the mechanism of charge carrier separation,[36,193] as schematically illustrated in Fig. 14: (a) the QD Schottky junction cell, (b) the depleted QD heterojunction cell, and (c) the QD-sensitized solar cell (QDSSC). Among these, QDHs are less important to Schottky-type devices, as charge carrier separation only occurs across a metal–semiconductor Schottky junction rather than at the heterointerface between two nanoscale semiconductors.

The semiconductor heterointerface in the depleted heterojunction and QDSSC device designs, which typically consists of a QD donor on a metal oxide acceptor (such as TiO_2), can be prepared through several methods, including post-synthetic deposition of the QDs to form a proximal heterostructure, chemical attachment with a molecular linker to form a linked heterostructure, or direct growth of the donor on the acceptor through a variety of procedures, as previously outlined in Section 2. The anticipation that more intimate, direct connections

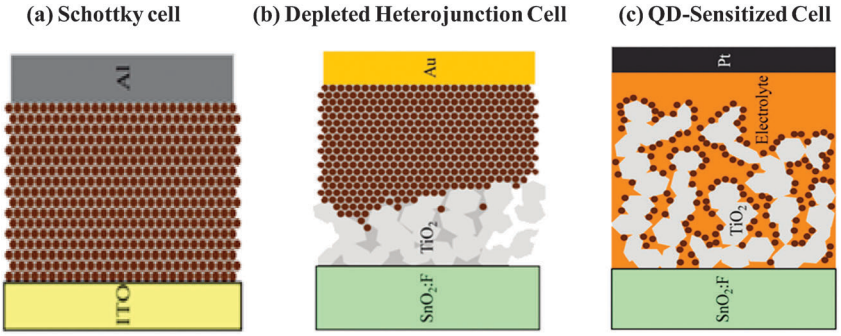

Fig. 14 Schematic diagrams of the three primary types of QD PV device: (a) the QD Schottky junction cell, (b) the depleted heterojunction cell, and (c) the QD-sensitized solar cell. Modified from ref. 193.

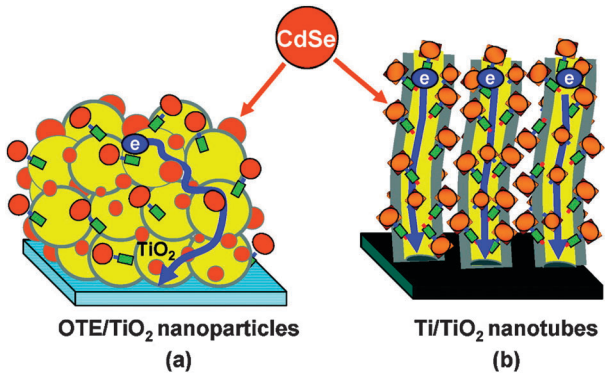

Fig. 15 Comparison of (a) a mesoporous TiO_2 NP film and (b) a TiO_2 NT array sensitized by CdSe QDs (from ref. 42).

between the donor and acceptor at the QDH will increase the rate and overall efficiency of charge carrier separation, as described in Section 4, motivates further study of QDH preparation in these QD-based PV devices.

Many procedures exist for the preparation of the acceptor material, as described in Section 2.2, with mesoporous metal oxide NP films being most common (Fig. 15a). Alternative acceptor morphologies,[194] such as electrochemically etched metal oxide NTs[86,87] and arrays of NWs,[50,51] have also been actively investigated and have been shown to impact the performance of the QD devices. For example, studies have confirmed the benefits of a 1D acceptor morphology by specifically comparing QDSSCs based on CdSe QDs linked by MPA to a TiO_2 NP film *versus* a TiO_2 NT array (Fig. 15). The QD-decorated TiO_2 NT array surpassed the TiO_2 NP film in efficiency. This example further illustrates that the 1D structure of TiO_2 NTs provides a direct path of conduction to the conductive substrate, improving charge carrier collection.[42]

As a direct analogue to the DSSC, which has been developed to the point of exhibiting impressive overall PV conversion efficiencies exceeding 12%,[195] the QDSSC is perhaps the most extensively explored QD-based solar energy conversion device design so far.[17,18,192] With the QD material serving as the absorber, its role is analogous to that of the dye in the DSSC: light absorption and exciton generation. Subsequent electron injection into the acceptor material achieves charge carrier separation. Because hole scavenging from the QDs remains the primary bottleneck in QDSSC performance, there have been numerous attempts to increase the efficiency of hole transfer, resulting in three major device configurations: solid-state heterojunction, inorganic–organic heterojunction, and liquid junction.[17,192] Because of the chemical incompatibility between the chalcogenide QD semiconductors used in QDSSCs and typical inorganic hole conductors, such as CuSCN[196] or CuI,[197] completely inorganic solid-state QDSSCs are less common.[192,198] However, successful incorporation of organic and polymer hole transporters, such as spiro-MeOTAD [2,2′,7,7′-tetrakis(*N*,*N*′-di-*p*-methoxyphenylamine)-9,9′-spirobifluorene][199] or poly(3-hexylthiophene) (P3HT),[198,200] respectively, encourages further development of the solid-state QDSSC design. Nevertheless, due to the ease of preparing uniform, conformal heterojunctions between a liquid electrolyte and the QD-sensitized wide-band gap semiconductor of the QDSSC, the liquid-junction configuration has become the preferred design, with the sulfide/polysulfide (S^{2-}/S_n^{2-}) redox couple and its analogues[113] consistently showing the best stability and highest PV conversion efficiencies.[17,201–203] While the iodide/triiodide (I^-/I_3^-) redox couple traditionally used with DSSCs has been incorporated into QDSSCs, the resulting device performance and long-term stability is inferior to S^{2-}/S_n^{2-}-based devices due to corrosion of the chalcogenide semiconductor.[18,201]

A more elaborate proposed use of QDHs is in the design of "rainbow" solar cells.[42] In such a device, ordered layers of QDs of different diameters could be assembled along a TiO_2 NT array (see Fig. 1) in such a sequence that sunlight will first reach QDs of the smallest diameter and, hence, the largest band gap. Longer wavelength photons will pass through the QD layers until reaching QDs large enough to have a band gap sufficiently small for long wavelength excitation. This design potentially enhances harvesting of the solar spectrum and reduces energy losses due to incomplete absorption, much as in the case of multi-junction solar cells (albeit different in how charge separation and collection is achieved).[42]

The performance of any QDH in a solar energy conversion device is determined by the combination of materials comprising the heterojunction, the synthetic method used to prepare the heterojunction,[204] and the heterostructure morphology, as it is these which most directly impact charge carrier separation at the heterointerface. The processes key to solar energy conversion

are light absorption, charge carrier separation at the heterointerface, charge transport through the donor and acceptor materials, and charge transfer at the various interfaces throughout the device. Rational design of QDHs considers three primary parameters: effectiveness, efficiency, and expense. Effective QDH solar energy conversion devices contain at least one semiconductor capable of absorbing solar photons with conduction and valence band edges positioned to form a type II band alignment with another semiconductor, facilitating charge separation. Efficient devices consider the electronic transport properties of each material along with the charge transfer mechanism at their interface, and they often leverage the unique advantages resulting from dimensional or morphological control at the nanoscale. Inexpensive devices demand earth-abundant materials, with a preference for materials of low toxicity; however, the benefits of nanoscale effects such as quantum confinement could outweigh concerns of cost and toxicity by maximizing device performance.

5.2 Examples of solar cells that use different QDH types

The three primary QDH types discussed in this review—proximally contacted, chemically linked, and epitaxial—have all been demonstrated in solar energy conversion devices. One example of a device design that employs proximal contact for charge separation is the PbSe QD-decorated ZnO NW cell.[50] As shown in Fig. 16a, this design incorporates a vertical array of ZnO NWs which provides a continuous conductive pathway to the conducting ITO-coated glass substrate. To prepare the QDHs, the ZnO NW-covered substrate is repeatedly dipped in a suspension of colloidal oleic acid-capped PbSe QDs, followed by dipping in a solution of 1,2-ethanedithiol, which exchanges with the oleic acid ligands and enables closer packing of the QDs, improving the efficiency of charge carrier transfer across the heterointerface and between QDs, as discussed above. The device is completed by depositing a gold top contact over a film of *N*,*N*′-bis(1-naphthalenyl)-*N*,*N*′-bis(phenylbenzidine) (α-NPD), an organic hole transporter. Although the likely primary charge transfer mechanism in such devices is hopping, due to the lack of epitaxial attachment or a molecular linker between the donor and acceptor, simple devices such as these are relatively easy to fabricate and use material dimensions to their advantage to show solar energy conversion efficiencies approaching 2%.[50]

QDs can also be chemically linked to the wide band gap metal oxide acceptor nanostructures, as depicted in Fig. 16b for a QDSSC consisting of an array of ZnO NWs synthesized on a FTO-coated glass substrate and photosensitized by chemical linkage of CdSe QDs with mercaptopropionic acid (MPA).[51] These QDHs on FTO-coated glass serve as the photoanode in this device configuration, with a thin film of Pt on FTO-coated glass serving as the cathode. A liquid electrolyte fills the interstitial spaces and completes the circuit of the device by providing a transport medium for the dissolved redox couple (I^-/I_3^-, in this case), which scavenges holes from the CdSe QDs and transports them to the cathode. This particular QDSSC design serves to highlight how a highly nanostructured acceptor material permits the formation of many quantum dot nanoscale heterostructures, increasing the fraction of incident light that can be harvested.[51] However, such QDSSCs featuring QDH formation through a chemical linker typically exhibit lower overall solar energy conversion efficiencies[103] due to relatively slow charge carrier transfer *via* a tunneling mechanism, as described in Section 4.

Following the reasoning and trends regarding charge carrier separation, an epitaxial connection between the QDH components could further improve the charge-transfer efficiency by providing a direct contact between the donor and acceptor with a high-quality shared interface. One system which meets this criterion is the PbS–TiO_2 QDH formed by the direct epitaxial growth of PbS QDs on a TiO_2 NP film deposited on an ITO-coated glass substrate through a doctor-blading procedure. As shown in Fig. 16c, solar cells were fabricated using these PbS–TiO_2 QDHs on ITO-coated glass as the working electrode. In lieu of a liquid electrolyte, a solid hole-transporting layer consisting of PbS QDs interconnected with MPA was spin-coated on the working electrode, in a design similar to that of the depleted heterojunction device (Fig. 14b), creating an all-inorganic, solid-state QD PV cell. Contact was made to the PbS QD layer with a sputtered thin film of Au–Pd. With this design, overall conversion efficiencies of 1.2% were achieved; clearly, then, further optimization of the other aspects of these devices is still needed.[68]

Highlighting the trend of increasing the QD-based PV device performance with improved contact and, hence, the charge

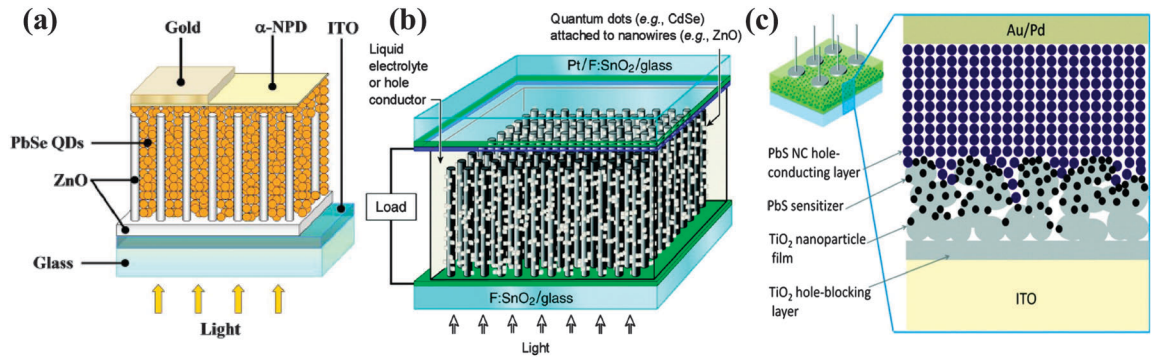

Fig. 16 Devices designed using heterojunctions formed by (a) proximally contacted PbSe QDs on ZnO NWs (from ref. 50), (b) CdSe QDs chemically linked to ZnO NWs by MPA (from ref. 51), and (c) epitaxial attachment of PbS QDs to a TiO_2 NP film (from ref. 68).

transfer between the donor and acceptor at the QDH, the highest-performing devices of today, which exhibit solar energy conversion efficiencies of about 5%, are usually prepared through a direct heterostructure growth technique, such as CBD or SILAR. In comparison, QDSSCs fabricated through post-synthesis assembly (*i.e.*, proximally contacted or chemically linked QDHs) typically show lower solar energy conversion efficiencies of 1–2%.[100,103,111,205] In order to achieve higher QDSSC conversion efficiency, it has been shown that the Mn^{2+} dopant species can be incorporated into CdS and CdSe QDs prepared on mesoporous TiO_2 NP films through SILAR.[202] The Mn^{2+} species creates midgap states in the QDs, and due to the slow Mn d–d transition ($^4T_1$–$^6A_1$), carrier lifetimes are substantially increased.[202] Direct contact with the acceptor facilitates separation and collection of the photoexcited charge carriers, and optimized devices exhibit overall conversion efficiencies of 5.4%. Similarly, recent examples of crystalline Sb_2S_3 (stibnite or antimonite) prepared *via* CBD on mesoporous TiO_2 acceptor films demonstrate the benefits of direct contact in the QDH.[198,199] The use of the spiro-MeOTAD organic hole-transporting material in conjunction with Sb_2S_3 films deposited over mesoporous TiO_2 films in extremely thin absorber solar cells yields PV devices with a solar conversion efficiency of 5.2%.[199] Additionally, P3HT has been demonstrated to be compatible with Sb_2S_3-sensitized mesoporous TiO_2 films to yield device efficiencies of 5.13%.[198] While these latter two examples are not strictly examples of QDH devices, they presently represent a target benchmark for QDH devices and serve to highlight the benefits of direct contact between donor and acceptor in achieving high efficiency.

6. Summary and perspectives

From materials combinations to synthetic strategies, the diversity of solution-grown quantum dot nanoscale heterostructures is impressive and rapidly expanding. By building upon and combining colloidal, hydrothermal, electrochemical, and vapor-phase synthetic techniques, researchers have developed novel methods of synthesizing QDHs through both direct growth and post-synthetic assembly. Upon examining this rapid expanding body of literature, it is very clear that QDHs composed of CdS and CdSe QDs on TiO_2, and to a lesser extent, PbS and PbSe QDs on TiO_2, have been most extensively investigated. This interest is likely due to the prominent roles of these model systems in QDSSCs and other QD-based solar energy conversion devices, as well as the abundance of highly developed and facile synthetic procedures for II–VI and lead salt QDs and TiO_2 nanostructures (the latter benefitting from the important role of TiO_2 nanostructures in the much more developed DSSC research field). This repetition and refinement has been of great benefit toward improving our fundamental understanding of charge transfer in nanoscale heterostructures and developing the characterization procedures, as discussed in this review. Some of these systems have also achieved success in efficient solar cell devices.

However, looking to the future, for QDHs to fully reach their potential for solar energy conversion, we must diversify the materials choices, particularly by using nanomaterials of more earth-abundant, low cost semiconductors,[206] such as pyrite (FeS_2),[207,208] Cu_2S,[209] hematite,[210] and/or more chemically complex nanomaterial phases, such as copper zinc tin sulfide (CZTS),[211–213] copper indium sulfide or selenide (CIS),[144,214–217] and others,[218,219] which have recently begun to emerge. New materials and material combinations would allow us to take full advantage of the material flexibility and low-cost processing techniques afforded by the QDHs, which are not available in bulk and thin film solar devices, as discussed in this review. While pairing similar synthetic methods for making the acceptor and donor structures in QDHs has been frequently successful, novel materials combinations may be possible by integrating dissimilar synthetic techniques. Finally, although epitaxial heterojunctions are more difficult to achieve using solution synthesis, they would be more robust and efficient than either proximal or chemically-linked junctions. The recent solution growth of heteroepitaxial PbSe QDs on earth-abundant hematite NWs[63] is an example of this strategy. Further research in these directions should bring new advances in the development of nanoscale heterostructures for efficient solar energy conversion.

Further fundamental studies of the physical properties of QDHs will allow us to identify, understand, and overcome the challenges in charge carrier transfer in nanostructures and help solar device design reach the next level. The differences between various synthetic, linking, and surface modification strategies to the charge transfer processes at the heterojunctions and other interfaces can be better understood using a diverse suite of physical characterization methods, such as time-resolved spectroscopy, surface sensitive nonlinear spectroscopy, terahertz spectroscopy, microwave photoconductivity spectroscopy, and temporally and spatially resolved surface photovoltage measurements. One interesting and unanswered question involves identifying the role and relative importance of coherent and incoherent charge transfer in suitably designed QDHs and how charge transfer can be influenced by heterostructure design and synthetic methods. These fundamental questions can be answered by the emerging methods of coherent multidimensional spectroscopy.

Finally, if we compare the QD and QDH solar devices discussed in this review with the second generation PV devices, current QD solar cell devices have not yet reached a competitive efficiency. We must emphasize that the QD PV technology has not yet reached the maturity of other technologies, and there are many critical factors and promising directions for creating high efficiency solar energy conversion devices. In comparison, DSSC and polymer solar cell technologies have been under development for two decades. However, it might also be the case that, if we want to take full advantage of QD solar cells and overcome the present efficiency bottlenecks, we will have to fully utilize the quantum mechanical effects that occur in QD solar cell designs. Although simple and cheap processing and fabrication are interesting and important motivations, they may not be sufficient to allow QD solar cells to surpass conventional PV devices in practical applications beyond certain niche applications. In order to realize this vision, we as a community

need to develop a deeper fundamental understanding of the unique quantum mechanical features in QD solar cells, such as hot electron transfer, coherent electron transfer, and multi-exciton generation, using state-of-the-art characterization technologies, enabling the design of QDH devices using more sophisticated (and likely novel) nanomaterials that leverage such features.

Acknowledgements

This research is supported by the U.S. Department of Energy, Office of Basic Energy Sciences, Division of Materials Sciences and Engineering, under Award DE-FG02-09ER46664. M.S.F. thanks the support of a NSF Graduate Research Fellowship. S.J. also thanks the Research Corporation SciaLog Award for Solar Energy Conversion for support.

References

1 N. S. Lewis, *Science*, 2007, **315**, 798–801.
2 N. S. Lewis and D. G. Nocera, *Proc. Natl. Acad. Sci. U. S. A.*, 2006, **103**, 15729–15735.
3 D. M. Adams, L. Brus, C. E. D. Chidsey, S. Creager, C. Creutz, C. R. Kagan, P. V. Kamat, M. Lieberman, S. Lindsay, R. A. Marcus, R. M. Metzger, M. E. Michel-Beyerle, J. R. Miller, M. D. Newton, D. R. Rolison, O. Sankey, K. S. Schanze, J. Yardley and X. Zhu, *J. Phys. Chem. B*, 2003, **107**, 6668–6697.
4 V. Balzani, A. Credi and M. Venturi, *ChemSusChem*, 2008, **1**, 26–58.
5 L. Carbone and P. D. Cozzoli, *Nano Today*, 2010, **5**, 449–493.
6 P. V. Kamat, *J. Phys. Chem. C*, 2008, **112**, 18737–18753.
7 P. D. Cozzoli, T. Pellegrino and L. Manna, *Chem. Soc. Rev.*, 2006, **35**, 1195–1208.
8 M. J. Bierman and S. Jin, *Energy Environ. Sci.*, 2009, **2**, 1050–1059.
9 P. V. Kamat, K. Tvrdy, D. R. Baker and J. G. Radich, *Chem. Rev.*, 2010, **110**, 6664–6688.
10 A. L. Fahrenbruch and R. H. Bube, *Fundamentals of Solar Cells*, Academic Press, New York, 1983.
11 C. A. Wolden, J. Kurtin, J. B. Baxter, I. Repins, S. E. Shaheen, J. T. Torvik, A. A. Rockett, V. M. Fthenakis and E. S. Aydil, *J. Vac. Sci. Technol., A*, 2011, **29**, 030801.
12 M. Gratzel, *Nature*, 2001, **414**, 338–344.
13 A. Hagfeldt, G. Boschloo, L. Sun, L. Kloo and H. Pettersson, *Chem. Rev.*, 2010, **110**, 6595–6663.
14 H. Weller, *Ber. Bunsen–Ges.*, 1991, **95**, 1361–1365.
15 R. Vogel, P. Hoyer and H. Weller, *J. Phys. Chem.*, 1994, **98**, 3183–3188.
16 P. Hoyer and R. Konenkamp, *Appl. Phys. Lett.*, 1995, **66**, 349–351.
17 P. V. Kamat, *Acc. Chem. Res.*, 2012, **45**, 1906–1915.
18 I. Mora-Sero and J. Bisquert, *J. Phys. Chem. Lett.*, 2010, **1**, 3046–3052.
19 M. G. Walter, E. L. Warren, J. R. McKone, S. W. Boettcher, Q. Mi, E. A. Santori and N. S. Lewis, *Chem. Rev.*, 2010, **110**, 6446–6473.
20 M. A. Green, *Third Generation Photovoltaics: Advanced Solar Energy Conversion*, Springer-Verlag, Berlin, 2003.
21 P. V. Kamat, *J. Phys. Chem. C*, 2007, **111**, 2834–2860.
22 G. W. Crabtree and N. S. Lewis, *Phys. Today*, 2007, **60**, 37–42.
23 G. F. Brown and J. Wu, *Laser Photonics Rev.*, 2009, **3**, 394–405.
24 W. Shockley and H. J. Queisser, *J. Appl. Phys.*, 1961, **32**, 510–519.
25 O. E. Semonin, J. M. Luther, S. Choi, H.-Y. Chen, J. Gao, A. J. Nozik and M. C. Beard, *Science*, 2011, **334**, 1530–1533.
26 J. B. Sambur, T. Novet and B. A. Parkinson, *Science*, 2010, **330**, 63–66.
27 J. A. McGuire, J. Joo, J. M. Pietryga, R. D. Schaller and V. I. Klimov, *Acc. Chem. Res.*, 2008, **41**, 1810–1819.
28 G. Nair, L.-Y. Chang, S. M. Geyer and M. G. Bawendi, *Nano Lett.*, 2011, **11**, 2145–2151.
29 G. Nair and M. G. Bawendi, *Phys. Rev. B: Condens. Matter Mater. Phys.*, 2007, **76**, 081304.
30 R. D. Schaller, M. Sykora, J. M. Pietryga and V. I. Klimov, *Nano Lett.*, 2006, **6**, 424–429.
31 W. A. Tisdale, K. J. Williams, B. A. Timp, D. J. Norris, E. S. Aydil and X. Y. Zhu, *Science*, 2010, **328**, 1543–1547.
32 A. J. Nozik, *Physica E (Amsterdam)*, 2002, **14**, 115–120.
33 A. J. Nozik, M. C. Beard, J. M. Luther, M. Law, R. J. Ellingson and J. C. Johnson, *Chem. Rev.*, 2010, **110**, 6873–6890.
34 D. J. Milliron, I. Gur and A. P. Alivisatos, *MRS Bull.*, 2005, **30**, 41–44.
35 W. U. Huynh, J. J. Dittmer and A. P. Alivisatos, *Science*, 2002, **295**, 2425–2427.
36 I. J. Kramer and E. H. Sargent, *ACS Nano*, 2011, **5**, 8506–8514.
37 R. Debnath, O. Bakr and E. H. Sargent, *Energy Environ. Sci.*, 2011, **4**, 4870–4881.
38 H. Lee, H. C. Leventis, S. J. Moon, P. Chen, S. Ito, S. A. Haque, T. Torres, F. Nuesch, T. Geiger, S. M. Zakeeruddin, M. Gratzel and M. K. Nazeeruddin, *Adv. Funct. Mater.*, 2009, **19**, 2735–2742.
39 B. H. Lee, K.-W. Kwon and M. Shim, *J. Mater. Chem.*, 2007, **17**, 1284–1291.
40 A. P. Alivisatos, *Science*, 1996, **271**, 933–937.
41 L. Brus, *J. Phys. Chem.*, 1986, **90**, 2555–2560.
42 A. Kongkanand, K. Tvrdy, K. Takechi, M. Kuno and P. V. Kamat, *J. Am. Chem. Soc.*, 2008, **130**, 4007–4015.
43 A. I. Hochbaum and P. Yang, *Chem. Rev.*, 2009, **110**, 527–546.
44 B. Tian, X. Zheng, T. J. Kempa, Y. Fang, N. Yu, G. Yu, J. Huang and C. M. Lieber, *Nature*, 2007, **449**, 885–889.
45 M. D. Kelzenberg, D. B. Turner-Evans, B. M. Kayes, M. A. Filler, M. C. Putnam, N. S. Lewis and H. A. Atwater, *Nano Lett.*, 2008, **8**, 710–714.
46 S. W. Boettcher, J. M. Spurgeon, M. C. Putnam, E. L. Warren, D. B. Turner-Evans, M. D. Kelzenberg,

J. R. Maiolo, H. A. Atwater and N. S. Lewis, *Science*, 2010, **327**, 185–187.
47 M. D. Kelzenberg, S. W. Boettcher, J. A. Petykiewicz, D. B. Turner-Evans, M. C. Putnam, E. L. Warren, J. M. Spurgeon, R. M. Briggs, N. S. Lewis and H. A. Atwater, *Nat. Mater.*, 2010, **9**, 239–244.
48 S. W. Boettcher, E. L. Warren, M. C. Putnam, E. A. Santori, D. Turner-Evans, M. D. Kelzenberg, M. G. Walter, J. R. McKone, B. S. Brunschwig, H. A. Atwater and N. S. Lewis, *J. Am. Chem. Soc.*, 2011, **133**, 1216–1219.
49 B. M. Kayes, H. A. Atwater and N. S. Lewis, *J. Appl. Phys.*, 2005, **97**, 114302.
50 K. S. Leschkies, A. G. Jacobs, D. J. Norris and E. S. Aydil, *Appl. Phys. Lett.*, 2009, **95**, 193103.
51 K. S. Leschkies, R. Divakar, J. Basu, E. Enache-Pommer, J. E. Boercker, C. B. Carter, U. R. Kortshagen, D. J. Norris and E. S. Aydil, *Nano Lett.*, 2007, **7**, 1793–1798.
52 M. J. Bierman, Y. K. A. Lau and S. Jin, *Nano Lett.*, 2007, **7**, 2907–2912.
53 M. J. Bierman, Y. K. A. Lau, A. V. Kvit, A. L. Schmitt and S. Jin, *Science*, 2008, **320**, 1060–1063.
54 Y. K. A. Lau, D. J. Chernak, M. J. Bierman and S. Jin, *J. Am. Chem. Soc.*, 2009, **131**, 16461–16471.
55 X. Chen and S. S. Mao, *Chem. Rev.*, 2007, **107**, 2891–2959.
56 K. Rajeshwar, N. R. de Tacconi and C. R. Chenthamarakshan, *Chem. Mater.*, 2001, **13**, 2765–2782.
57 I. Robel, M. Kuno and P. V. Kamat, *J. Am. Chem. Soc.*, 2007, **129**, 4136–4137.
58 A. Zur and T. C. Mcgill, *J. Appl. Phys.*, 1984, **55**, 378–386.
59 V. A. Shchukin, N. N. Ledentsov and D. Bimberg, *Epitaxy of Nanostructures*, Springer-Verlag, New York, 2004.
60 J. W. Matthews and A. E. Blakeslee, *J. Cryst. Growth*, 1974, **27**, 118–125.
61 L. J. Lauhon, M. S. Gudiksen and C. M. Lieber, *Philos. Trans. R. Soc., A*, 2004, **362**, 1247–1260.
62 Y. K. A. Lau, D. J. Chernak, M. J. Bierman and S. Jin, *J. Mater. Chem.*, 2009, **19**, 934–940.
63 R. S. Selinsky, S. Shin, M. A. Lukowski and S. Jin, *J. Phys. Chem. Lett.*, 2012, **3**, 1649–1656.
64 R. Agarwal, *Small*, 2008, **4**, 1872–1893.
65 J. W. Elam, N. P. Dasgupta and F. B. Prinz, *MRS Bull.*, 2011, **36**, 899–906.
66 F. P. Zamborini, A. J. Mieszawska, R. Jalilian and G. U. Sumanasekera, *Small*, 2007, **3**, 722–756.
67 R. Costi, A. E. Saunders and U. Banin, *Angew. Chem., Int. Ed.*, 2010, **49**, 4878–4897.
68 K. P. Acharya, E. Khon, T. O'Conner, I. Nemitz, A. Klinkova, R. S. Khnayzer, P. Anzenbacher and M. Zamkov, *ACS Nano*, 2011, **5**, 4953–4964.
69 J. R. Mann and D. F. Watson, *Langmuir*, 2007, **23**, 10924–10928.
70 D. Liu and P. V. Kamat, *J. Phys. Chem.*, 1993, **97**, 10769–10773.
71 B. O'Regan, J. Moser, M. Anderson and M. Graetzel, *J. Phys. Chem.*, 1990, **94**, 8720–8726.
72 R. Plass, S. Pelet, J. Krueger, M. Gratzel and U. Bach, *J. Phys. Chem. B*, 2002, **106**, 7578–7580.
73 L. Etgar, J. Park, C. Barolo, M. K. Nazeeruddin, G. Viscardi and M. Graetzel, *ACS Appl. Mater. Interfaces*, 2011, **3**, 3264–3267.
74 K. Tvrdy, P. A. Frantsuzov and P. V. Kamat, *Proc. Natl. Acad. Sci. U. S. A.*, 2011, **108**, 29–34.
75 J. J. H. Pijpers, R. Koole, W. H. Evers, A. J. Houtepen, S. Boehme, C. D. Donega, D. Vanmaekelbergh and M. Bonn, *J. Phys. Chem. C*, 2010, **114**, 18866–18873.
76 H. C. Leventis, F. O'Mahony, J. Akhtar, M. Afzaal, P. O'Brien and S. A. Haque, *J. Am. Chem. Soc.*, 2010, **132**, 2743–2750.
77 M. A. Hossain, J. R. Jennings, Z. Y. Koh and Q. Wang, *ACS Nano*, 2011, **5**, 3172–3181.
78 J. Park, J. Joo, S. G. Kwon, Y. Jang and T. Hyeon, *Angew. Chem., Int. Ed.*, 2007, **46**, 4630–4660.
79 E. Palomares, J. N. Clifford, S. A. Haque, T. Lutz and J. R. Durrant, *J. Am. Chem. Soc.*, 2003, **125**, 475–482.
80 G. Ai, W. T. Sun, X. F. Gao, Y. L. Zhang and L. M. Peng, *J. Mater. Chem.*, 2011, **21**, 8749–8755.
81 Y. Tak, S. J. Hong, J. S. Lee and K. Yong, *J. Mater. Chem.*, 2009, **19**, 5945–5951.
82 J. Cai, J. Ye, S. Chen, X. Zhao, D. Zhang, S. Chen, Y. Ma, S. Jin and L. Qi, *Energy Environ. Sci.*, 2012, **5**, 7575–7581.
83 C. Cheng and H. J. Fan, *Nano Today*, 2012, **7**, 327–343.
84 P. Roy, S. Berger and P. Schmuki, *Angew. Chem., Int. Ed.*, 2011, **50**, 2904–2939.
85 G. K. Mor, O. K. Varghese, M. Paulose, K. Shankar and C. A. Grimes, *Sol. Energy Mater. Sol. Cells*, 2006, **90**, 2011–2075.
86 W.-T. Sun, Y. Yu, H.-Y. Pan, X.-F. Gao, Q. Chen and L.-M. Peng, *J. Am. Chem. Soc.*, 2008, **130**, 1124–1125.
87 X. F. Gao, H. B. Li, W. T. Sun, Q. Chen, F. Q. Tang and L. M. Peng, *J. Phys. Chem. C*, 2009, **113**, 7531–7535.
88 X. F. Gao, W. T. Sun, Z. D. Hu, G. Ai, Y. L. Zhang, S. Feng, F. Li and L. M. Peng, *J. Phys. Chem. C*, 2009, **113**, 20481–20485.
89 W. Zhang and S. Yang, *Acc. Chem. Res.*, 2009, **42**, 1617–1627.
90 M. A. Lukowski and S. Jin, *J. Phys. Chem. C*, 2011, **115**, 12388–12395.
91 J. B. Mooney and S. B. Radding, *Annu. Rev. Mater. Sci.*, 1982, **12**, 81–101.
92 L. M. Peter, K. G. U. Wijayantha, D. J. Riley and J. P. Waggett, *J. Phys. Chem. B*, 2003, **107**, 8378–8381.
93 Y. Li, X.-Y. Yang, Y. Feng, Z.-Y. Yuan and B.-L. Su, *Crit. Rev. Solid State Mater. Sci.*, 2012, **37**, 1–74.
94 J. G. Lu, P. Chang and Z. Fan, *Mater. Sci. Eng., R*, 2006, **52**, 49–91.
95 J. T. Yates Jr, *Surf. Sci.*, 2009, **603**, 1605–1612.
96 D. F. Wang, H. G. Zhao, N. Q. Wu, M. A. El Khakani and D. L. Ma, *J. Phys. Chem. Lett.*, 2010, **1**, 1030–1035.
97 C. Wang, K.-W. Kwon, M. L. Odlyzko, B. H. Lee and M. Shim, *J. Phys. Chem. C*, 2007, **111**, 11734–11741.
98 K. R. Gopidas, M. Bohorquez and P. V. Kamat, *J. Phys. Chem.*, 1990, **94**, 6435–6440.
99 L. Spanhel, H. Weller and A. Henglein, *J. Am. Chem. Soc.*, 1987, **109**, 6632–6635.

100 S. Gimenez, I. Mora-Sero, L. Macor, N. Guijarro, T. Lana-Villarreal, R. Gomez, L. J. Diguna, Q. Shen, T. Toyoda and J. Bisquert, *Nanotechnology*, 2009, **20**, 295204.
101 Z.-J. Zhou, J.-q. Fan, X. Wang, W.-Z. Sun, W.-H. Zhou, Z.-L. Du and S.-X. Wu, *ACS Appl. Mater. Interfaces*, 2011, **3**, 2189–2194.
102 I. Gur, N. A. Fromer, M. L. Geier and A. P. Alivisatos, *Science*, 2005, **310**, 462–465.
103 D. F. Watson, *J. Phys. Chem. Lett.*, 2010, **1**, 2299–2309.
104 N. Guijarro, T. Lana-Villarreal, I. Mora-Sero, J. Bisquert and R. Gomez, *J. Phys. Chem. C*, 2009, **113**, 4208–4214.
105 D. R. Pernik, K. Tvrdy, J. G. Radich and P. V. Kamat, *J. Phys. Chem. C*, 2011, **115**, 13511–13519.
106 P. R. Yu, K. Zhu, A. G. Norman, S. Ferrere, A. J. Frank and A. J. Nozik, *J. Phys. Chem. B*, 2006, **110**, 25451–25454.
107 B. R. Hyun, Y. W. Zhong, A. C. Bartnik, L. F. Sun, H. D. Abruna, F. W. Wise, J. D. Goodreau, J. R. Matthews, T. M. Leslie and N. F. Borrelli, *ACS Nano*, 2008, **2**, 2206–2212.
108 Y. M. Sung, J. C. Lee, T. G. Kim and H. J. Choi, *Appl. Phys. Lett.*, 2007, **91**, 113104.
109 L. Liu, J. Hensel, R. C. Fitzmorris, Y. Li and J. Z. Zhang, *J. Phys. Chem. Lett.*, 2010, **1**, 155–160.
110 D. Lawless, S. Kapoor and D. Meisel, *J. Phys. Chem.*, 1995, **99**, 10329–10335.
111 I. Robel, V. Subramanian, M. Kuno and P. V. Kamat, *J. Am. Chem. Soc.*, 2006, **128**, 2385–2393.
112 J. B. Sambur, S. C. Riha, D. Choi and B. A. Parkinson, *Langmuir*, 2010, **26**, 4839–4847.
113 L. Li, X. C. Yang, J. J. Gao, H. N. Tian, J. Z. Zhao, A. Hagfeldt and L. C. Sun, *J. Am. Chem. Soc.*, 2011, **133**, 8458–8460.
114 J. C. Kim, J. Choi, Y. B. Lee, J. H. Hong, J. I. Lee, J. W. Yang, W. I. Lee and N. H. Hur, *Chem. Commun.*, 2006, 5024–5026.
115 B. R. Hyun, A. C. Bartnik, L. F. Sun, T. Hanrath and F. W. Wise, *Nano Lett.*, 2011, **11**, 2126–2132.
116 X.-Y. Yu, B.-X. Lei, D.-B. Kuang and C.-Y. Su, *Chem. Sci.*, 2011, **2**, 1396–1400.
117 A. Zaban, O. I. Micic, B. A. Gregg and A. J. Nozik, *Langmuir*, 1998, **14**, 3153–3156.
118 K. P. Acharya, N. N. Hewa-Kasakarage, T. R. Alabi, I. Nemitz, E. Khon, B. Ullrich, P. Anzenbacher and M. Zamkov, *J. Phys. Chem. C*, 2010, **114**, 12496–12504.
119 K. P. Acharya, T. R. Alabi, N. Schmall, N. N. Hewa-Kasakarage, M. Kirsanova, A. Nemchinov, E. Khon and M. Zamkov, *J. Phys. Chem. C*, 2009, **113**, 19531–19535.
120 S. Yamamoto, T. Kendelewicz, J. T. Newberg, G. Ketteler, D. E. Starr, E. R. Mysak, K. J. Andersson, H. Ogasawara, H. Bluhm, M. Salmeron, G. E. Brown and A. Nilsson, *J. Phys. Chem. C*, 2010, **114**, 2256–2266.
121 S. Jin, M. J. Bierman and S. A. Morin, *J. Phys. Chem. Lett.*, 2010, **1**, 1472–1480.
122 H. Pathan and C. Lokhande, *Bull. Mater. Sci.*, 2004, **27**, 85–111.
123 O. Niitsoo, S. K. Sarkar, C. Pejoux, S. Ruhle, D. Cahen and G. Hodes, *J. Photochem. Photobiol., A*, 2006, **181**, 306–313.
124 X. F. Gao, W. T. Sun, G. Ai and L. M. Peng, *Appl. Phys. Lett.*, 2010, **96**, 153104.
125 S. Q. Huang, Q. X. Zhang, X. M. Huang, X. Z. Guo, M. H. Deng, D. M. Li, Y. H. Luo, Q. Shen, T. Toyoda and Q. B. Meng, *Nanotechnology*, 2010, **21**, 375201.
126 S. W. Jung, J. H. Park, W. Lee, J. H. Kim, H. Kim, C. J. Choi and K. S. Ahn, *J. Appl. Phys.*, 2011, **110**, 054301.
127 H. Wang, Y. Bai, H. Zhang, Z. Zhang, J. Li and L. Guo, *J. Phys. Chem. C*, 2010, **114**, 16451–16455.
128 S.-Q. Fan, D. Kim, J.-J. Kim, D. W. Jung, S. O. Kang and J. Ko, *Electrochem. Commun.*, 2009, **11**, 1337–1339.
129 Z.-X. Li, Y.-L. Xie, H. Xu, T.-M. Wang, Z.-G. Xu and H.-L. Zhang, *J. Photochem. Photobiol., A*, 2011, **224**, 25–30.
130 Y. Tak, S. J. Hong, J. S. Lee and K. Yong, *Cryst. Growth Des.*, 2009, **9**, 2627–2632.
131 Y. Zhang, T. Xie, T. Jiang, X. Wei, S. Pang, X. Wang and D. Wang, *Nanotechnology*, 2009, **20**, 155707.
132 W. Lee, S. K. Min, V. Dhas, S. B. Ogale and S.-H. Han, *Electrochem. Commun.*, 2009, **11**, 103–106.
133 C. Chen, G. Ali, S. H. Yoo, J. M. Kum and S. O. Cho, *J. Mater. Chem.*, 2011, **21**, 16430–16435.
134 G. Zhu, L. Pan, T. Xu and Z. Sun, *ACS Appl. Mater. Interfaces*, 2011, **3**, 1472–1478.
135 Y. Xie, G. Ali, S. H. Yoo and S. O. Cho, *ACS Appl. Mater. Interfaces*, 2010, **2**, 2910–2914.
136 C. B. Murray, D. J. Norris and M. G. Bawendi, *J. Am. Chem. Soc.*, 1993, **115**, 8706–8715.
137 A. Braga, S. Gimenez, I. Concina, A. Vomiero and I. Mora-Sero, *J. Phys. Chem. Lett.*, 2011, **2**, 454–460.
138 H. Lee, M. K. Wang, P. Chen, D. R. Gamelin, S. M. Zakeeruddin, M. Gratzel and M. K. Nazeeruddin, *Nano Lett.*, 2009, **9**, 4221–4227.
139 T.-L. Li, Y.-L. Lee and H. Teng, *Energy Environ. Sci.*, 2012, **5**, 5315–5324.
140 N. Guijarro, T. Lana-Villarreal, Q. Shen, T. Toyoda and R. Gomez, *J. Phys. Chem. C*, 2010, **114**, 21928–21937.
141 M. A. Hossain, Z. Y. Koh and Q. Wang, *Phys. Chem. Chem. Phys.*, 2012, **14**, 7367–7374.
142 M. A. Hossain, J. R. Jennings, N. Mathews and Q. Wang, *Phys. Chem. Chem. Phys.*, 2012, **14**, 7154–7161.
143 S. S. Mali, S. K. Desai, S. S. Kalagi, C. A. Betty, P. N. Bhosale, R. S. Devan, Y.-R. R. Ma and P. S. Patil, *Dalton Trans.*, 2012, **41**, 6130–6136.
144 M. Berruet, M. Valdes, S. Cere and M. Vazquez, *J. Mater. Sci.*, 2012, **47**, 2454–2460.
145 S. Gavrilov, I. Oja, B. Lim, A. Belaidi, W. Bohne, E. Strub, J. Rohrich, M. C. Lux-Steiner and T. Dittrich, *Phys. Status Solidi A*, 2006, **203**, 1024–1029.
146 B. Ghosh, S. Chowdhury, P. Banerjee and S. Das, *Thin Solid Films*, 2011, **519**, 3368–3372.
147 S. B. Bubenhofer, C. M. Schumacher, F. M. Koehler, N. A. Luechinger, R. N. Grass and W. J. Stark, *J. Phys. Chem. C*, 2012, **116**, 16264–16270.
148 Q. Dai, J. Chen, L. Lu, J. Tang and W. Wang, *Nano Lett.*, 2012, **12**, 4187–4193.
149 K. Rajeshwar, *Adv. Mater.*, 1992, **4**, 23–29.

150 W.-C. Kwak, S.-H. Han, T. G. Kim and Y.-M. Sung, *Cryst. Growth Des.*, 2010, **10**, 5297–5301.
151 X.-Y. Yu, J.-Y. Liao, K.-Q. Qiu, D.-B. Kuang and C.-Y. Su, *ACS Nano*, 2011, **5**, 9494–9500.
152 S. Banerjee, S. K. Mohapatra, P. P. Das and M. Misra, *Chem. Mater.*, 2008, **20**, 6784–6791.
153 H. Zhang, X. Quan, S. Chen, H. Yu and N. Ma, *Chem. Mater.*, 2009, **21**, 3090–3095.
154 C. Wang, L. Sun, H. Yun, J. Li, Y. Lai and C. Lin, *Nanotechnology*, 2009, **20**.
155 X. Wang, H. Zhu, Y. Xu, H. Wang, Y. Tao, S. Hark, X. Xiao and Q. Li, *ACS Nano*, 2010, **4**, 3302–3308.
156 W. Wang, Q. Zhao, K. Laurent, Y. Leprince-Wang, Z.-M. Liao and D. Yu, *Nanoscale*, 2012, **4**, 261–268.
157 J.-C. Lee, T. G. Kim, W. Lee, S.-H. Han and Y.-M. Sung, *Cryst. Growth Des.*, 2009, **9**, 4519–4523.
158 N. P. Dasgupta, H. J. Jung, O. Trejo, M. T. McDowell, A. Hryciw, M. Brongersma, R. Sinclair and F. B. Prinz, *Nano Lett.*, 2011, **11**, 934–940.
159 Y. Xu and M. A. A. Schoonen, *Am. Miner.*, 2000, **85**, 543–556.
160 J. Jasieniak, M. Califano and S. E. Watkins, *ACS Nano*, 2011, **5**, 5888–5902.
161 R. W. Meulenberg, J. R. I. Lee, A. Wolcott, J. Z. Zhang, L. J. Terminello and T. van Buuren, *ACS Nano*, 2009, **3**, 325–330.
162 J. A. Cina and G. R. Fleming, *J. Phys. Chem. A*, 2004, **108**, 11196–11208.
163 G. S. Engel, T. R. Calhoun, E. L. Read, T. K. Ahn, T. Mancal, Y. C. Cheng, R. E. Blankenship and G. R. Fleming, *Nature*, 2007, **446**, 782–786.
164 G. R. Fleming and G. D. Scholes, *Nature*, 2004, **431**, 256–257.
165 G. D. Scholes, G. R. Fleming, A. Olaya-Castro and R. van Grondelle, *Nat. Chem.*, 2011, **3**, 763–774.
166 Q. Shen, K. Katayama, M. Yamaguchi, T. Sawada and T. Toyoda, *Thin Solid Films*, 2005, **486**, 15–19.
167 N. A. Anderson and T. Q. Lian, *Annu. Rev. Phys. Chem.*, 2005, **56**, 491–519.
168 L. Dworak, V. V. Matylitsky, M. Braun and J. Wachtveitl, *Phys. Rev. Lett.*, 2011, **107**, 247401.
169 N. N. Hewa-Kasakarage, P. Z. El-Khoury, A. N. Tarnovsky, M. Kirsanova, I. Nemitz, A. Nemchinov and M. Zamkov, *ACS Nano*, 2010, **4**, 1837–1844.
170 A. V. Pisliakov, M. F. Gelin and W. Domcke, *J. Phys. Chem. A*, 2003, **107**, 2657–2666.
171 X. Ai, N. Anderson, J. Guo, J. Kowalik, L. M. Tolbert and T. Lian, *J. Phys. Chem. B*, 2006, **110**, 25496–25503.
172 W. R. Duncan and O. V. Prezhdo, *Annu. Rev. Phys. Chem.*, 2007, **58**, 143–184.
173 R. S. Dibbell and D. F. Watson, *J. Phys. Chem. C*, 2009, **113**, 3139–3149.
174 J. S. Nevins, K. M. Coughlin and D. F. Watson, *ACS Appl. Mater. Interfaces*, 2011, **3**, 4242–4253.
175 R. S. Dibbell, D. G. Youker and D. F. Watson, *J. Phys. Chem. C*, 2009, **113**, 18643–18651.
176 Y. Yang, W. Rodriguez-Cordoba, X. Xiang and T. Lian, *Nano Lett.*, 2012, **12**, 303–309.
177 Y. Tachibana, K. Umekita, Y. Otsuka and S. Kuwabata, *J. Phys. Chem. C*, 2009, **113**, 6852–6858.
178 B. C. Fitzmorris, G. K. Larsen, D. A. Wheeler, Y. Zhao and J. Z. Zhang, *J. Phys. Chem. C*, 2012, **116**, 5033–5041.
179 E. Canovas, P. Moll, S. A. Jensen, Y. A. Gao, A. J. Houtepen, L. D. A. Siebbeles, S. Kinge and M. Bonn, *Nano Lett.*, 2011, **11**, 5234–5239.
180 A. V. Pakoulev, S. B. Block, L. A. Yurs, N. A. Mathew, K. M. Kornau and J. C. Wright, *J. Phys. Chem. Lett.*, 2010, **1**, 822–828.
181 J. C. Wright, *Annu. Rev. Phys. Chem.*, 2011, **62**, 209–230.
182 L. A. Yurs, S. B. Block, A. V. Pakoulev, R. S. Selinsky, S. Jin and J. Wright, *J. Phys. Chem. C*, 2011, **115**, 22833–22844.
183 L. A. Yurs, S. B. Block, A. V. Pakoulev, R. S. Selinsky, S. Jin and J. Wright, *J. Phys. Chem. C*, 2012, **116**, 5546–5553.
184 S. B. Block, L. A. Yurs, A. V. Pakoulev, R. S. Selinsky, S. Jin and J. Wright, *J. Phys. Chem. Lett.*, 2012, **3**, 2707–2712.
185 L. Kronik and Y. Shapira, *Surf. Sci. Rep.*, 1999, **37**, 1–206.
186 O. O. Ekiz, K. Mizrak and A. Dana, *ACS Nano*, 2010, **4**, 1851–1860.
187 E. M. Barea, M. Shalom, S. Gimenez, I. Hod, I. Mora-Sero, A. Zaban and J. Bisquert, *J. Am. Chem. Soc.*, 2010, **132**, 6834–6839.
188 I. Mora-Sero, J. Bisquert, T. Dittrich, A. Belaidi, A. S. Susha and A. L. Rogach, *J. Phys. Chem. C*, 2007, **111**, 14889–14892.
189 D. G. Cahill and R. J. Hamers, *J. Vac. Sci. Technol., B: Microelectron. Nanometer Struct.–Process., Meas., Phenom.*, 1991, **9**, 564–567.
190 R. J. Hamers and K. Markert, *Phys. Rev. Lett.*, 1990, **64**, 1051–1054.
191 S. Jin and T. Lian, *Nano Lett.*, 2009, **9**, 2448–2454.
192 G. Hodes and D. Cahen, *Acc. Chem. Res.*, 2012, **45**, 705–713.
193 A. G. Pattantyus-Abraham, I. J. Kramer, A. R. Barkhouse, X. H. Wang, G. Konstantatos, R. Debnath, L. Levina, I. Raabe, M. K. Nazeeruddin, M. Gratzel and E. H. Sargent, *ACS Nano*, 2010, **4**, 3374–3380.
194 T. Toyoda and Q. Shen, *J. Phys. Chem. Lett.*, 2012, **3**, 1885–1893.
195 A. Yella, H. W. Lee, H. N. Tsao, C. Y. Yi, A. K. Chandiran, M. K. Nazeeruddin, E. W. G. Diau, C. Y. Yeh, S. M. Zakeeruddin and M. Gratzel, *Science*, 2011, **334**, 629–634.
196 B. O'Regan, F. Lenzmann, R. Muis and J. Wienke, *Chem. Mater.*, 2002, **14**, 5023–5029.
197 P. M. Sirimanne and H. Tributsch, *J. Solid State Chem.*, 2004, **177**, 1789–1795.
198 J. A. Chang, J. H. Rhee, S. H. Im, Y. H. Lee, H. J. Kim, S. I. Seok, M. K. Nazeeruddin and M. Gratzel, *Nano Lett.*, 2010, **10**, 2609–2612.
199 S. J. Moon, Y. Itzhaik, J. H. Yum, S. M. Zakeeruddin, G. Hodes and M. Gratzel, *J. Phys. Chem. Lett.*, 2010, **1**, 1524–1527.
200 P. P. Boix, Y. H. Lee, F. Fabregat-Santiago, S. H. Im, I. Mora-Sero, J. Bisquert and S. I. Seok, *ACS Nano*, 2011, **6**, 873–880.

201 G. Hodes, *J. Phys. Chem. C*, 2008, **112**, 17778–17787.
202 P. K. Santra and P. V. Kamat, *J. Am. Chem. Soc.*, 2012, **134**, 2508–2511.
203 V. Chakrapani, D. Baker and P. V. Kamat, *J. Am. Chem. Soc.*, 2011, **133**, 9607–9615.
204 S. Gimenez, T. Lana-Villarreal, R. Gomez, S. Agouram, V. Munoz-Sanjose and I. Mora-Sero, *J. Appl. Phys.*, 2010, **108**, 064310.
205 H. J. Lee, J.-H. Yum, H. C. Leventis, S. M. Zakeeruddin, S. A. Haque, P. Chen, S. I. Seok, M. Graetzel and M. K. Nazeeruddin, *J. Phys. Chem. C*, 2008, **112**, 11600–11608.
206 C. Wadia, A. P. Alivisatos and D. M. Kammen, *Environ. Sci. Technol.*, 2009, **43**, 2072–2077.
207 C. Wadia, Y. Wu, S. Gul, S. K. Volkman, J. Guo and A. P. Alivisatos, *Chem. Mater.*, 2009, **21**, 2568–2570.
208 M. Caban-Acevedo, M. S. Faber, Y. Tan, R. J. Hamers and S. Jin, *Nano Lett.*, 2012, **12**, 1977–1982.
209 Y. Wu, C. Wadia, W. Ma, B. Sadtler and A. P. Alivisatos, *Nano Lett.*, 2008, **8**, 2551–2555.
210 L. Li, Y. Yu, F. Meng, Y. Tan, R. J. Hamers and S. Jin, *Nano Lett.*, 2012, **12**, 724–731.
211 G. M. Ford, Q. Guo, R. Agrawal and H. W. Hillhouse, *Chem. Mater.*, 2011, **23**, 2626–2629.
212 Q. Guo, H. W. Hillhouse and R. Agrawal, *J. Am. Chem. Soc.*, 2009, **131**, 11672–11673.
213 S. C. Riha, B. A. Parkinson and A. L. Prieto, *J. Am. Chem. Soc.*, 2009, **131**, 12054–12055.
214 S. K. Batabyal, L. Tian, N. Venkatram, W. Ji and J. J. Vittal, *J. Phys. Chem. C*, 2009, **113**, 15037–15042.
215 K.-T. Kuo, D.-M. Liu, S.-Y. Chen and C.-C. Lin, *J. Mater. Chem.*, 2009, **19**, 6780–6788.
216 D. Pan, X. Wang, Z. H. Zhou, W. Chen, C. Xu and Y. Lu, *Chem. Mater.*, 2009, **21**, 2489–2493.
217 M. E. Norako and R. L. Brutchey, *Chem. Mater.*, 2010, **22**, 1613–1615.
218 A. M. Wiltrout, N. J. Freymeyer, T. Machani, D. P. Rossi and K. E. Plass, *J. Mater. Chem.*, 2011, **21**, 19286–19292.
219 M. E. Norako, M. J. Greaney and R. L. Brutchey, *J. Am. Chem. Soc.*, 2012, **134**, 23–26.